University of West Bohemia
Faculty of Applied Sciences
Department of Mechanics

Master Thesis

Biomechanical Study of Sacral Bone Fixation Techniques

Plzeň, 2017 Jana Hartlová

I hereby declare that this thesis is my own work, and it does not contain other people's work without this being stated; and that the bibliography contains all the literature that I have used in writing the thesis, and that all references refer to this bibliography.

Plzeň, 30 May 2017 Jana Hartlová

Acknowledgment

First of all, I would like to express my gratitude to my supervisor Ing. Libor Lobovský, Ph.D., for the guidance, continuous support, a great deal of patience, motivation and his friendly approach over the last four years.

I would like to thank Ing. Tomáš Mandys, Ph.D., Ing. Vladimír Lukeš, Ph.D, and Ing. Alena Jonášová, Ph.D., for their help with the preparation of finite element model.

My thanks go to MUDr. Martin Salášek, Ph.D., who assisted in planning and realisation of the experimental study and who provided me with great knowledge in the field of pelvic anatomy and sacral bone fractures. I would like to thank Ing. Jan Krystek, Ph.D., for his assistance in the experimental measurements.

Finally, I owe my deepest gratitude to my family and my boyfriend, for their endless support and patience.

This work was supported by the project SGS-2016-059.

Abstract

The thesis is focused on a unilateral transforaminal sacral fracture. An experimental study, performed on orthopaedic solid-foam pelvic models, was realised to investigate the response of the pelvic model to mechanical loading. The models were tested in the intact state, the fractured state and the fractured state after surgical stabilisation using internal fixators. A finite element model of intact pelvis and fractured pelvis was designed and validated based on a set of experimental data and information on the properties of the solid-foam model.

Keywords
pelvis, sacrum, fracture, digital image correlation, finite element model, transiliac internal fixator, iliosacral screw, transiliac plate, sacral bar

Abstrakt

V rámci diplomové práce byla studována jednostranná transforaminální zlomenina křížové kosti a možnosti její stabilizace pomocí vnitřních fixátorů. V experimentální části studie realizované na ortopedických modelech lidské pánve bylo sledováno chování pánve při zatěžování v intaktním stavu, ve stavu po vytvoření zlomeniny a ve stavu po stabilizaci zlomeniny pomocí vybraných fixačních technik. V rámci konečněprvkové studie byl na základě experimentálních dat a informací o testovaném ortopedickém modelu vytvořen a validován konečněprvkový model intaktní lidské pánve a pánve s transforaminální zlomeninou.

Klíčová slova

lidská pánev, křížová kost, zlomenina, digitální korelace obrazu, metoda konečných prvků, transiliakální vnitřní fixátor, iliosakrální šroub, transiliakální dlaha, sakrální tyč

Table of contents

List of figures

List of tables

Introduction

Unstable fractures in pelvic area are very challenging for surgeons as they are often associated with many complications and possible late effects. The appropriate and urgent medical care, together with the selection of the most suitable fixation is the key factor for successful treatment and minimization of potential negative consequences.

This thesis is focused on a study of a unilateral transforaminal sacral fracture and methods of its operative management. Many different types of fixation techniques might be used for the stabilisation of this type of fracture; their suitability has to be assessed individually for each patient with respect to their health state, severity of associated injuries and potential complications resulting from application of the particular fixation technique. Another important criterion in the evaluation of suitability of given fixation technique is its biomechanical behaviour and a level of stability provided to the fractured bone, which is the subject of the experimental study presented in this thesis.

The mechanical response of pelvis was investigated in the intact state, the fractured state, and the fractured state after surgical reduction and stabilisation by particular fixation technique. The behaviour of pelvis in all the states was tested experimentally and the intact and the fractured state was a subject of a finite element study.

The experimental part of the research was performed using the orthopaedic solid-foam pelvic models. Their use was convenient in this type of study; their principal advantage for the experiments is that all the models are identical in size, shape and material, which ensures the repeatability of the measurements under the same conditions. Contrary to that, results of studies performed on cadaveric pelves are strongly affected by the variance in size and material properties of particular bones. Furthermore, the models are made of homogeneous and isotropic material, which enabled the application of simple and reliable material model in the performed finite element analysis.

In the finite element study, the model of human pelvis was designed and validated based on the data from experimental measurements and their setup. Geometry of the solid-foam pelvic model was obtained from computed tomography scans of the solid-foam model. The material properties of the solid foam were determined in a series of experimental measurements.

The biomechanical stability of ten internal sacral fracture fixation techniques was studied in experimental measurements performed on the above mentioned solid-foam models. The techniques utilised four types of fixation devices. Specifically, the mechanically tested pelvic models were treated by the transiliac internal fixator, the iliosacral screw, the transiliac plate, the sacral bar, and their combinations. For the data acquisition and processing during the experimental measurements, a multi-camera digital image correlation system was used.

The main body of the thesis is structured into four chapters. The first chapter provides anatomic and orthopaedic background to studied fracture and fixation techniques. One section is focused on review of former studies on management of dorsal pelvic ring injuries.

In the second chapter, the description of the experimental procedure is provided. Properties of the solid-foam pelvic model are presented, including the information on its material parameters. Afterwards, the course of the measurements and the methods of data processing and evaluation are described.

In the third chapter, the finite element study is presented. It provides the results of experimental measurements used for the validation of the finite element model. The preparation of the finite element model, the definition of the problem and the obtained results are desbribed in this chapter.

The fourth chapter is focused on the experimental study on sacral bone fixation techniques. The techniques are divided into groups according to the utilised fixation devices. Within these groups, several criteria describing the behaviour of each technique are discussed and compared.

1 Sacral Bone Fractures

Pelvic fractures are quite uncommon when compared to fractures of other bones in human body, they represent 3 % to 8 % of all fractures [7]. However, they belong to the most challenging injuries which require a lot of practical experience for the surgeons to feel competent in treating this kind of injuries [9].

Pelvic fractures seldom occur as the only injury; most of times pelvic fractures occur among polytraumatised patients, very often it is a consequence of high-energy injuries – traffic accidents or falls from a great height [6]. These data are confirmed by real-patient information published in various studies. For instance, Chen et al. [21] reviewed 58 patients with unstable posterior pelvic ring fracture. Injury of 38 patients was a consequence of traffic accident, 17 patients fell from height and in 3 cases it was a result from other type of crush. In study presented by Dienstknecht et al. [12] medical cases of 67 patients with dorsal pelvic ring injury were reported while 30 of the injuries were a consequence of motor vehicle accidents and 26 were caused by falls from heights. Furthermore, only 7 patients had solely the pelvic injury while the 60 remaining suffered multiple injuries in other body parts. These high-energy injuries are more dangerous and serious in comparison to low-energy injuries as they mostly lead to unstable fractures which generally require operative reduction and fixation.

The mortality rate at patients sustaining pelvic fractures is estimated to be around 5 % [7]. Moreover, fracture of pelvis may result in wide range of severe life-threatening complications or permanent consequences. The severity and high level danger is caused by the incidence of many important tissues and viscera in pelvic area such as the spinal cord and the osteoligamentous, neurovascular, and urogenital structures. Rotationally or vertically unstable fractures may lead to issues with locomotion.

Fortunately for patients, significant improvements in prehospital care increase the chances of successful treatment [9]. In other words, many patients who previously would have died before transport to the hospital due to severe unstable pelvic fractures are nowadays successfully brought to the operating room. This progress results in increased number and advanced complexity of performed surgeries as more heavily injured patients are operated.

1.1 Pelvic Anatomy

The pelvis is a ring of bones located in the lower torso. It is connected to the lumbar spine in the upper part and to femora in the lower part. The most significant functions of pelvis are bearing the weight of upper body and the support and protection of viscera and other tissues located in the pelvic cavity, especially the inner reproductive organs and the urinary track. Its structure and shape specific for humans enables an upright posture and the bipedal locomotion [1].

Pelvis consists of several bones, some of which fuse with age to form more rigid pelvic bone. The anterior and lateral view of pelvis with the description of individual bones is provided in Fig. 1.1. The particular bones which form pelvis are two coxal bones, the sacral bone and the coccyx. Their description is provided below [2, 3].

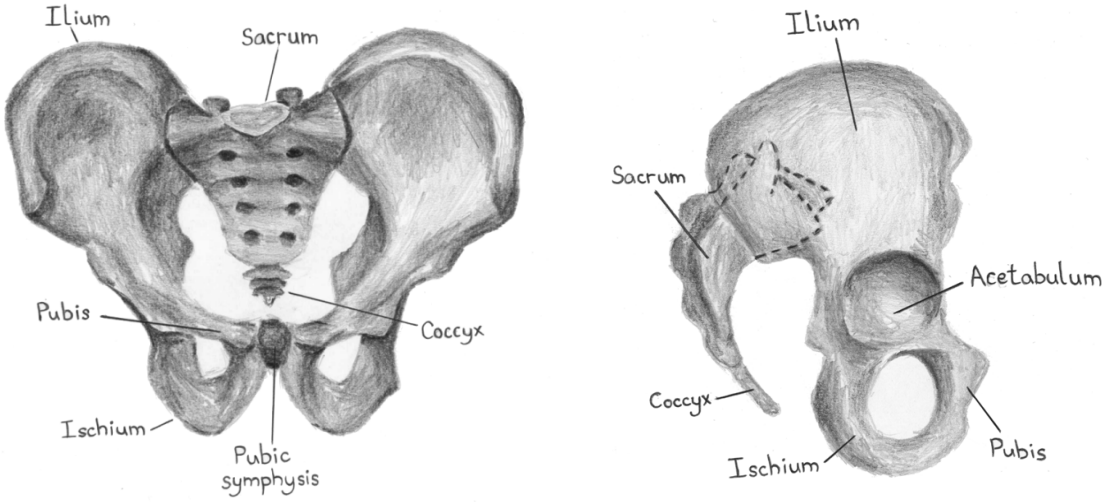

Fig. 1.1: The anterior (left) and lateral (right) view of pelvis with the description of the individual pelvic bones.

1.1.1 Os coxae

Ossa coxae, also called hip bones or coxal bones are paired, irregularly shaped bones. Each coxal bone is formed by three fused bones (See Fig. 1.1). The largest one is the ilium. It is the most superior, wide flat bone located lateral to the sacrum. The second bone, the ischium, is the posterior inferior part of the os coxae. This bone supports the body weight in the sitting position. Pubis, which is the smallest one, is located in the anterior part. The pubic bones are attached to the pubic symphysis. These three bones meet in a large circular depression called the acetabulum which forms the socket for the hip joint.

The coxal bones are joined together in the anterior part of pelvis by a cartilaginous, slightly movable joint called pubic symphysis. Pubic symphysis in female pelvis is thicker and more flexible, which, together with softer articulations during pregnancy and different shape of pelvic bones, provides larger space for childbirth. In the posterior part, coxal bones are attached to the sacral bone by the sacroiliac joints.

1.1.2 Os sacrum

Os sacrum, or the sacral bone, is a wedge shaped synostosis of five vertebrae (See Fig. 1.2). These become fused in the adulthood by around the age of 30, however there are visible transverse ridges which denote the primary division. The sacral canal, a continuation

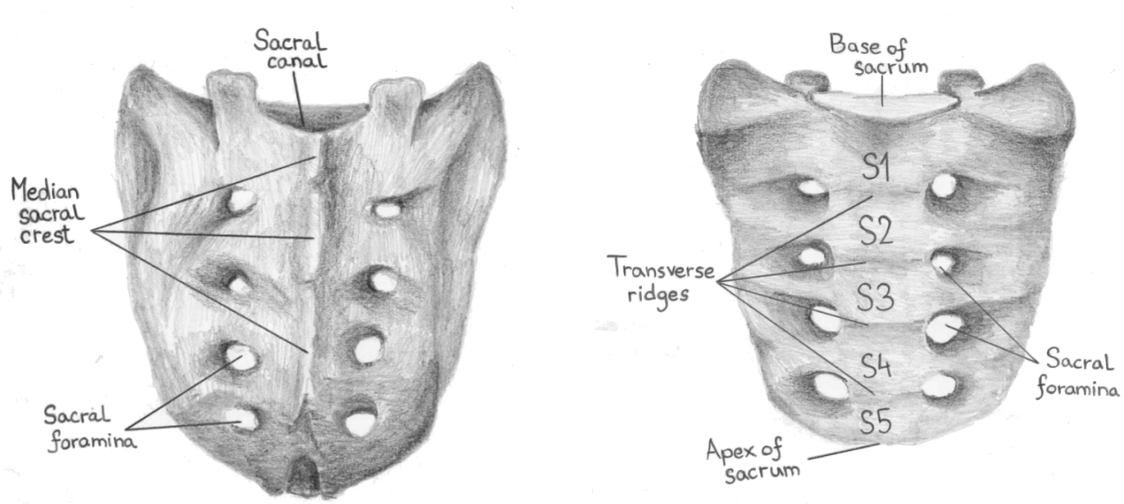

Fig. 1.2: The posterior (left) and anterior (right) view of sacrum.

of the spinal canal through which the spinal cord and nerves pass, runs throughout the sacrum. Its walls are perforated by the anterior and posterior sacral foramina on the both sides of the median sacral crest. These openings, occurring between every pair of spinal vertebrae, allow number of structures such as spinal nerves, spinal artery or transforaminal ligaments to pass through.

On the lateral sides the sacrum is connected to coxal bones by very tight sacroiliac joints. The movement in these joints is further reduced by many ligaments which make the pelvic structure stiffer. At the base of sacrum, the sacrum is connected to the fifth lumbar vertebra by a lumbosacral joint. Its apex articulates with the coccyx.

1.1.3 Os coccygis

Os coccygis, also referred to as the coccyx or the tailbone, is the smallest and the most interior part of spine. Similarly to the sacrum it is a synostosis of three to five vertebrae. Until the end of puberty, these vertebrae are made of cartilage tissue which slowly ossifies to form individual bones. Later in adulthood they fuse to form a single coccyx. The functions of the coccyx are muscle attachment, shock absorption during sitting and spinal cord support.

1.2 Studied Fracture

The fracture being studied within this thesis is a unilateral transforaminal sacral fracture (see Fig 1.3). According to three widely used classification systems, the studied fracture is classified as follows:

- type II in Denis Three-zone Classification,
- part of C1 fracture in Marvin Tile's classification, only the posterior pelvic ring is disrupted,
- 61-C1.3 in AO/OTA classification.

Detailed classification of pelvic fractures is provided in [4].

Based on the results of study published in [12], sacral fracture was incident in 51 of 67 reviewed patients who suffered some type of dorsal pelvic ring injury requiring reduction and stabilisation. Denis type II fracture was incident in 32 cases, which represents 48 %

of all dorsal pelvic ring injuries. The remaining injuries were following: sacroiliac displacement (occurring in 16 patients), Denis type I fracture (17 patients) and Denis type III fracture (2 patients).

When the transforaminal sacral fracture is the only pelvic injury, it results in rotational instability. Thus, in order to restore the stability, the pelvis requires surgical reduction and stabilisation. Many different approaches and fixation techniques were developed and utilized. Nowadays, less invasive techniques are favoured as they reduce the damage of surrounding soft tissues and the entire fracture region. Current surgical techniques allow the precise bone positioning and faster healing.

The suitability of any fixation technique cannot be stated in general, it has to be carefully reviewed for each particular patient with respect to their health condition and all potential risks as well as the difficulties associated with application of given fixation technique.

1.3 Fixation Techniques and Devices

Within the scope of conducted study, ten fixation techniques for internal fixation of previously described sacral fracture were studied and compared. Four types of fixation devices were used for this purpose. Their list and description is provided below.

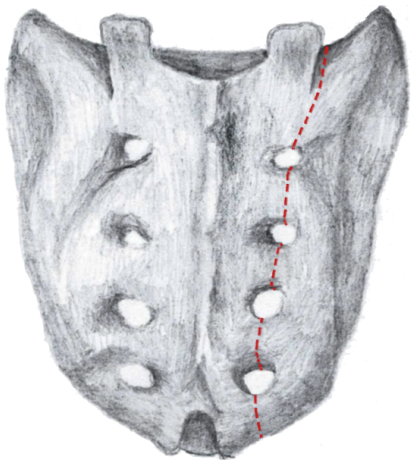

Fig. 1.3: Studied fracture illustrated on dorsal surface of sacrum.

1.3.1 Studied fixation devices

1.3.1.1 Transiliac internal fixator

Transiliac internal fixator (TIFI, Fig. 1.4) allows a minimally invasive stabilisation which minimizes the disorder of surrounding tissue while it keeps the risk of wound infections low [13]. It consists of two locking head pedicle screws and a connection rod. The screws are inserted into the alae of ilium and they are connected by the rod so that the devices forms a fixed-angle construction [19].

This provides angular stable fixation suitable for unstable unilateral injuries of dorsal pelvic ring – dislocations in sacroiliac joints and fractures of sacrum. Conversely, TIFI is not applicable for fractures involving the area of alae of ilium or seriously damaged soft tissues in gluteal region. In case of bilateral sacral fracture, TIFI is applicable only when combined with another type of fixation device such as iliosacral screw [11].

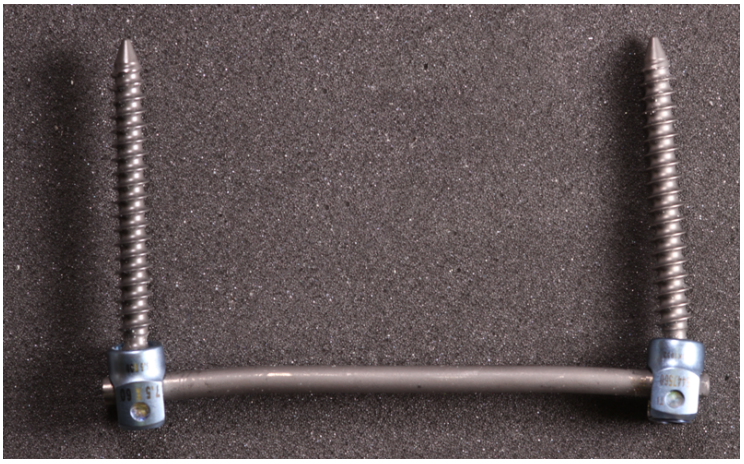

Fig. 1.4: Transiliac internal fixator

1.3.1.2 Iliosacral screw

Iliosacral screw (ISS) is very commonly used fixation device [8], however, its application is associated with many potential complications [14]. The screw is applied through the ala of ilium into the first (S1), eventually the second (S2) sacral vertebra. As one screw does not provide rotational stability to the fractured bone, two screws are gerenally inserted.

The screws can be either fully threaded (Fig. 1.5) or partially threaded (Fig. 1.6). The process of application is challenging process which requires accuracy and great knowledge

of inner composition of affected sacral vertebra. The screw must be inserted into the so-called "safe screw channel" or "transsacral channel" [17] so as not to injure nerves passing through sacrum. The positioning and dimensions of channel differs significantly at each particular patient, at some people the channels might not be sufficient for screw placement, or the maximal diameter or inserted screw is limited [8].

During insertion it is necessary to use a navigation to guide the fixation. Before the surgery, high quality computed tomography (CT) of pelvis is acquired together with x-rays of sacrum and S1, eventually S2. These data might be sufficient for precise insertion, however, some hospitals use real time information during screw insertion obtained from imaging methods, such image intensifier fluoroscopy or intraoperative navigation based on infrared light [18].

ISS is suitable for stabilisation of sacroiliac joint dislocations and well aligned vertical sacral fractures – both unilateral and bilateral. Contraindication to ISS application is neurological deficit in sacral fractures, insufficient bone quality, large uncorrected displacement of sacral fracture or poor quality transsacral channel disallowing the screw insertion [16].

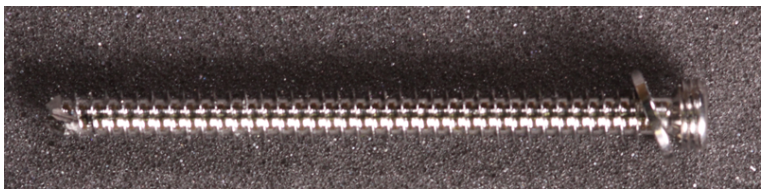

Fig. 1.5: Fully threaded iliosacral screw.

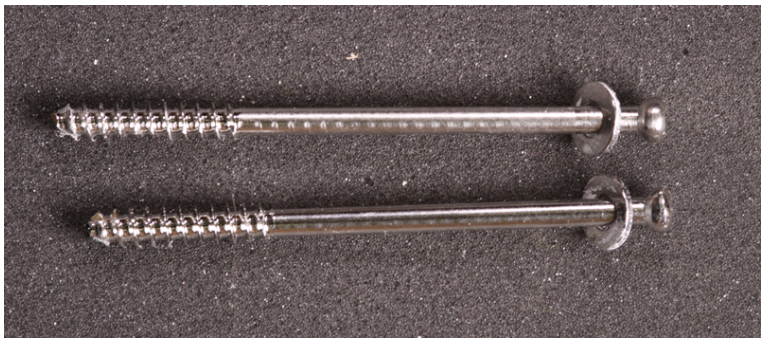

Fig. 1.6: Partially threaded iliosacral screw.

1.3.1.3 Transiliac plate

Transiliac plate (TP), also called ilioiliac plate, is a metal plate with holes distributed along its whole length (Fig. 1.7). These holes are intended for screw insertion. Dynamic compression plate was used within the performed study. Between each pair of holes there is a deep notch on both edges which allows the plate to be bent in all directions. The plate has to be long enough to reach from one iliac wing to the other one.

Before the application of TP it is necessary to bend the plate according to size and shape of patient's pelvis. Thin bending templates are shaped along the alae of ilium. Based on their shape, the TP is bent so as to fit precisely the particular pelvis. After positioning, the plate is attached to ilia using 2-4 screws.

TP is advantageous to use for stabilisation of fractures with large comminuted zones as it allows bridging the zones. Furthermore, it is applicable in case of selected central sacral fractures and unstable sacral fracture, both unilateral and bilateral. The contraindication for TP is poor state of surrounding soft tissue [16].

Fig. 1.7: Transiliac plate.

1.3.1.4 Sacral bar

Sacral bar (SB), also named as iliosacral bar, transiliac bar or sacral rod is a continuously threated rod (Fig. 1.8). Nowadays this device is not frequently used as the only fixation technique due to lower biomechanical stability and possible opening of the fracture due to position of the fixation point which is posterior to the fracture level [10]. Its another

disadvantage is high risk of excessive compression along the fracture line which is not desirable.

During application, SB is drilled through the alae of ilium and fixed on both external sides by two nuts to prevent loosening.

Indication for application of SB is unilateral sacroiliac dislocation and unilateral sacral fracture. Contraindication for use of SB is bilateral unstable sacral fracture [11].

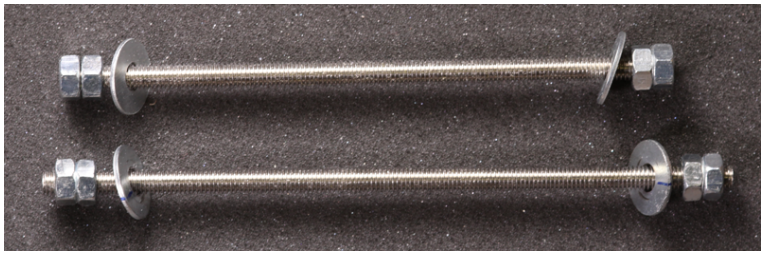

Fig. 1.8: Sacral bar.

1.3.2 Studied fixation techniques

Ten fixation techniques presented in Fig. 1.9 were tested in this study. A single TIFI was tested in two locations. In the first case (supraacetabular positioning), it was placed in level of superior posterior iliac spine – (Fig. 1.9a), in the second case (classical positioning) it was applied approximately 3 cm cranially to the superior posterior iliac spine (Fig. 1.9b). Afterwards, biomechanical properties of dual TIFI (Fig. 1.9c), one in the classical position and the second in the supraacetabular position, were examined.

Two ways of positioning of a dual partially threaded ISS were studied. Firstly, the screws were inserted into the S1 vertebra, in the plane parallel to the plane of sacral base (see Fig. 1.9d). Secondly, the screws were inserted in the S1. Both of them were positioned in a plane perpendicular to the sacral base plane, one was located more cranially (see Fig. 1.9e).

A combination of a supraacetabular TIFI and a single ISS inserted into the S1 vertebra (Fig. 1.9f) was tested in two modifications. The partially threaded ISS was used in the first case, and the fully threaded ISS was used in the second case.

Two measurements studied the behaviour of a dual SB. The cranial SB was positioned in the level of L5/S1 vertebrae, the caudal SB was distant approximately 3 cm (Fig. 1.9g).

The measurement with the same positioning of SB was conducted twice in order to study the influence of level of compression in the fracture line area.

Two types of fixation techniques using TP were studied. Firstly, a single TP was positioned in the same location as the classical TIFI (Fig. 1.9h). Secondly, a dual TP was tested with the position of the plates matching the positions of fixators in dual TIFI technique (Fig. 1.9i).

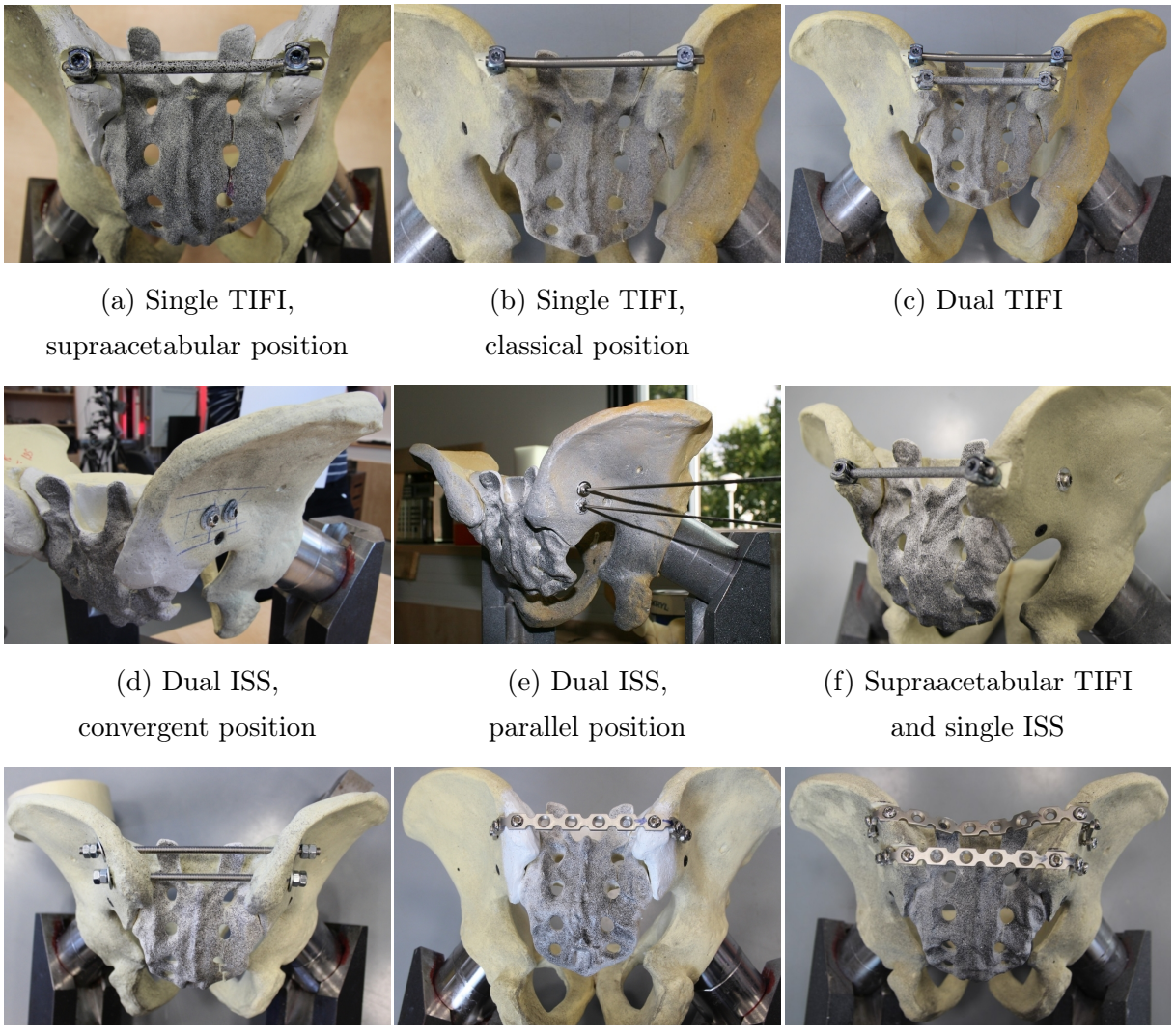

(a) Single TIFI, supraacetabular position

(b) Single TIFI, classical position

(c) Dual TIFI

(d) Dual ISS, convergent position

(e) Dual ISS, parallel position

(f) Supraacetabular TIFI and single ISS

(g) Dual SB

(h) Single TP

(i) Dual TP

Fig. 1.9: Studied fixation techniques.

1.3.3 Former studies on sacral bone fixation techniques

Many studies investigating behaviour and biomechanical properties of particular sacral fracture fixation devices and techniques and comparing them were conducted in the past. However, most of the comparative studies deal only with limited amount of techniques, usually comparing two or three techniques. Outcomes of studies dealing with fixation techniques investigated in this thesis are presented below.

Füchtmeier et al. [19] presented the first study on TIFI. He describes a prospective study of 31 patients whose injuries were treated by TIFI and comes to conclusion that TIFI is suitable for sacral fractures and sacroiliac joint injuries as it provides sufficient biomechanical stability and the risks associated with its application are low. Specifically, following complications were observed: 5 patients suffered from pain when lying, 2 developed a wound infection and in 1 had a screw loosening.

Another studies on TIFI were introduced by Dienstknecht et al. [12, 13]. In [12] 67 patients who suffered either sacroiliac displacement or sacral fracture were reviewed in 7 years after surgery where TIFI was utilised to stabilise the dorsal pelvic ring. Wound infection affected 4 patients, in 1 case the screw loosened and 1 patient had screw malpositioning caused by an iatrogenesis.

The second study of Dienstknecht et al. presented in [13] is focused on biomechanical properties of TIFI and its comparison to two ISS and two ventral dynamic compression plates. Six cadaveric pelves were utilised within the study while each fixation device was tested on each pelvis. The pelves were fixed in one acetabulum and cyclically loaded through sacral base with force equivalent to 70 % of body mass. Movement of selected points on the pelvic surface was detected. The study comes to conclusion that the differences in biomechanical stability of those tested devices are not significant and it denotes TIFI as adequate alternative for stabilisation of dorsal pelvic ring injuries.

Gorczyca et al. [20] performed an experimental comparison of two ISS and two SB on eight cadaveric pelves when treating vertically unstable sacral fracture. During measurement the pelves were supported in both acetabula and cyclically loaded until failure of the fixation technique. The load was applied at the fifth lumbar vertebra at a rate of 10 mm/s. At each model, both techniques were subsequently tested. When applied as the first fixation technique on particular pelvis, SB shows 30 % higher strength than ISS; when applied as second fixation the difference in strength was negligible. These results

suggest that there is no advantage in favouring the widely used ISS over SB in terms of biomechanical stability provided to the fractured bone.

An extensive study comparing nine clinically used fixation techniques suitable for stabilisation of unilateral sacroiliac joint dislocation was performed by Yinger et al. [15]. ISS, SB, anterior sacroiliac joint plate and posterior tension band plate were tested in various combinations. The fixation techniques studied by Yinger et al. that are reflected in this study are two ISS and two SB. The measurements performed by Yinger et al. were realised on six plastic models which were rigidly mounted in one acetabula where femur and system simulating abductor muscles were attached. They were cyclically loaded through sacrum to 1000 N. Each fixation technique was tested on each model while the order of their application remained the same. Gap opening at the fracture location and enabled rotation of the hemipelvis were recorded. Based on these criteria, 2 ISS achieved better results and demonstrated higher stiffness – in case of 2 SB, the sacroiliac gap was approximately 80 % larger and the rotation was 50 % larger than when 2 ISS were applied.

In study by Chen et al. [21] it is presented the review of 58 patients who had the unstable posterior pelvic ring fracture treated either by a single TP (29 patients) or by a dual ISS (29 patients). There was no incidence of fixator failure and no infection related to the surgery. Two patients treated with ISS had an injury of sacral nerves as a consequence of ISS application. The functional evaluation score was very similar for both techniques. According to Majeed functional score [23], patients achieved very similar results. In case of ISS, 10 patients got excellent, 16 good and 3 fair, in case of TP results of 9 patients were excellent, 16 were good and 4 were fair. The mean duration of surgery was 26.6 % lower for ISS and the patients were exposed to more than 7 times lower radiation dose from x-ray examinations. On the other hand, the average blood loss was more than two times higher in comparison to application of TP. Other advantage of TP over ISS was higher mechanical strength of posterior pelvic ring observed at patients having the fracture stabilised by TP.

Suzuki et al. [22] presented a retrospective clinical study of 19 patients who had either unilateral (14 patients) or bilateral (5 patients) sacral fracture treated by TP. Considering the incidence of bilateral fractures, which means that one patient suffered two fractures of the sacrum, Dennis type II facture occurred in 20 cases, Dennis type I in 2 and Dennis type III also in 2 cases. Wound infection as a consequence of surgery occurred in 2 patients. The mean residual displacement after surgery was 5 mm while in 9 patients it was graded as excellent, in 7 patients as good and in 3 as fair. Based on Majeed functional

score [23, 22], the overall results of 5 patients were graded as excellent, 8 as good, 4 as fair and 1 as poor.

Each of the above mentioned studies bring information about a particular set of fixation techniques; however, their outcomes are generally not mutually comparable as they were realised in different way under different conditions. Therefore, the principal aim of the study presented in this thesis was to provide a direct comparison of biomechanical properties of ten fixation techniques suitable for treatment of unstable vertical sacral fracture.

2 Experimental Analysis

The objective of this chapter is to provide the comprehensive description of the whole experimental procedure performed for the purpose of the assessment of biomechanical behaviour of selected fixation techniques.

During the whole procedure, the emphasis was placed on assurance of identical conditions for testing of each fixation in order to assess the repeatability and comparability. For this purpose, solid-foam models were used instead of cadaveric pelves which are commonly used in other biomechanical studies. As the pelvic size, shape, bone quality and material properties differ significantly among people, the usage of cadaveric pelves brings high uncertainty into the outcomes. Contrary to that, plastic pelvic models are all produced with the same geometry from the same material, which makes their use advantageous in this type of study.

2.1 Pelvic models

Orthopaedic hard plastic models of male pelvis made of solid foam were utilised in the study. A separate model was used for each tested technique, which eliminated the potential influence of previous tests on quality of the model and results obtained for the subsequently tested techniques. There was, however, one exception to this rule, when dual TIFI and single TIFI were consecutively tested on one pelvic model as the latter technique was prepared simply by removing one TIFI from the former one. The material of the models was considered to be homogeneous and isotropic.

2.1.1 Material properties

Material properties of the pelvic models – Young's modulus and Poisson's ratio – were established in a series of experimental measurements performed at NTIS - New Technologies for the Information Society research centre [28]. Cuboidal specimens were cut out of the plastic models. The dimensions of the cuboids were selected so as to be suitable for the uniaxial tensile test. The cross-section had the average size 8.14 × 3.74 mm, the average length was 67.8 mm.

2.1.1.1 Experimental determination of Young's modulus

39 specimens were subjected to the displacement controlled tensile testing in the materials testing machine ZWICK ROELL Z050. The specimens were placed in the testing machine and were slowly stretched until failure (See Fig. 2.1). The crosshead velocity was set to 5 mm/min, the initial distance between grips was 40 mm, and the initial distance between the two extensometers attached to the central part of the specimen was 20 mm. The strain was measured in terms of data obtained from the extensometers.

The stress-strain curves of all specimens are shown in Fig. 2.2. Linear part of the curve corresponding to the strain 0.3-0.5 %, was approximated by straight line. The interval was selected according to ASTM D3039 testing specification. This interval is indicated by

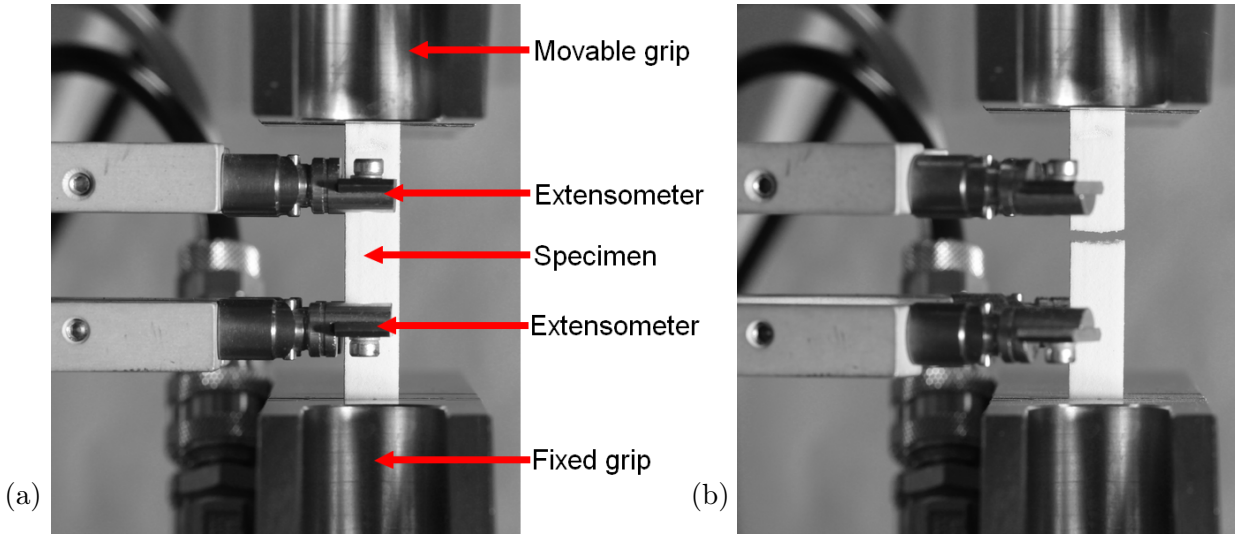

Fig. 2.1: The experimental measurement of Young's modulus. (a) The experimental setup, (b) the specimen after failure.

light red rectangle in the figure. Based on the tangent of this line, the Young's modulus was determined for each experiment. The mean value of Young's modulus of all models equals 194 ± 28 MPa.

2.1.1.2 Experimental determination of Poisson's ratio

The Poisson's ratio was determined based on the controlled tensile testing of twenty specimens. Digital image correlation (DIC) method was utilised for the data evaluation. The detailed description of its principle is presented in Section 2.3. The surface of the specimen was covered by random black and white pattern. During the measurement, images were acquired capturing the change of specimen's shape. The pattern allowed to trace the displacements of particular points on the surface based on their positions in the individual pictures.

The value of the Poisson's ratio was computed as a ratio of transverse strain to axial strain in the central part of the specimen. Based on the preliminary analysis of experimental data, the Poisson's ratio of the tested solid foam material was estimated equal to 0.2.

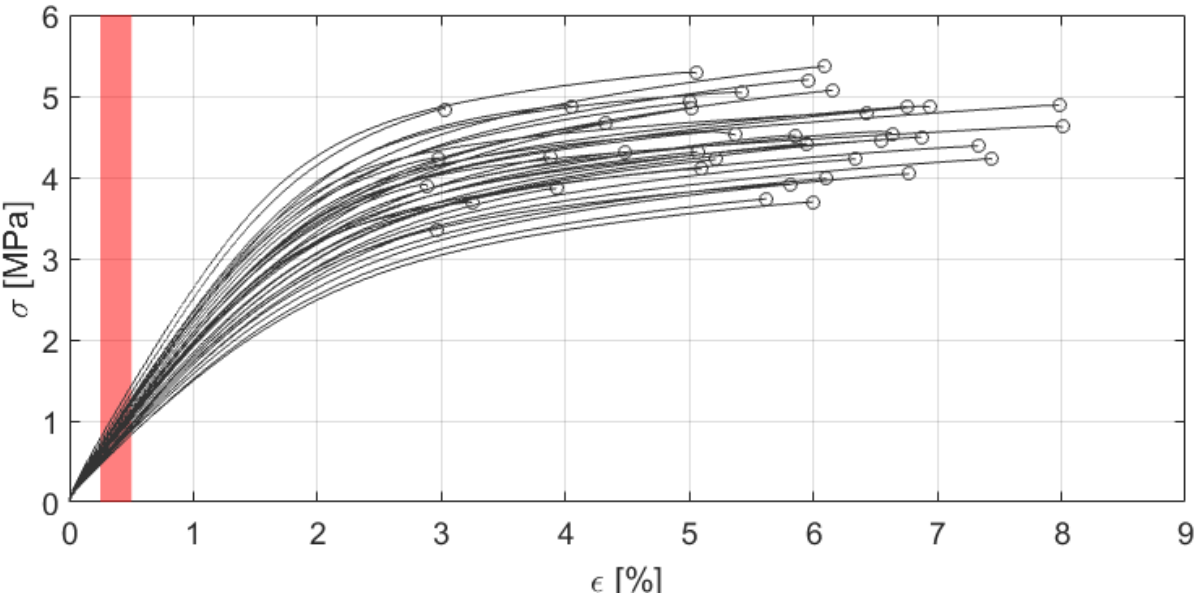

Fig. 2.2: The stress-strain curve obtained from uniaxial tensile tests. End of each measurement – the moment of material failure – is marked by circle. The light red rectangle indicates the part of the curve used for the computation of Young's modulus.

2.2 Experimental Workflow

2.2.1 Preliminary operations

During all the experiments, the same sequence of operations was realised. First of all, the model was rigidly mounted on the metal stand designed and manufactured specially for the pelvic models utilised in this study. The model was fixed in acetabula so that no movement was allowed. In comparison pelvis in physiological position of human body, the pelvic model was rotated in the mid-sagittal plane so that the base of sacrum was positioned horizontally. As DIC was used to record the course of the measurements and to evaluate the results, the sacral surface was covered by random black and white pattern.

The model was subjected to the force controlled testing in the materials testing machine. The load was applied in vertical direction at the sacral base via a cuboidal compressive element with the 1.5×1.5 cm square-shaped cross section. So as to distribute the applied force to the whole surface of sacral base, a specially designed metal plate was put between the model and the compressive element. Its upper surface was flat while the lower one accurately copied the irregular surface of sacral base. The setup is displayed in Fig. 2.3.

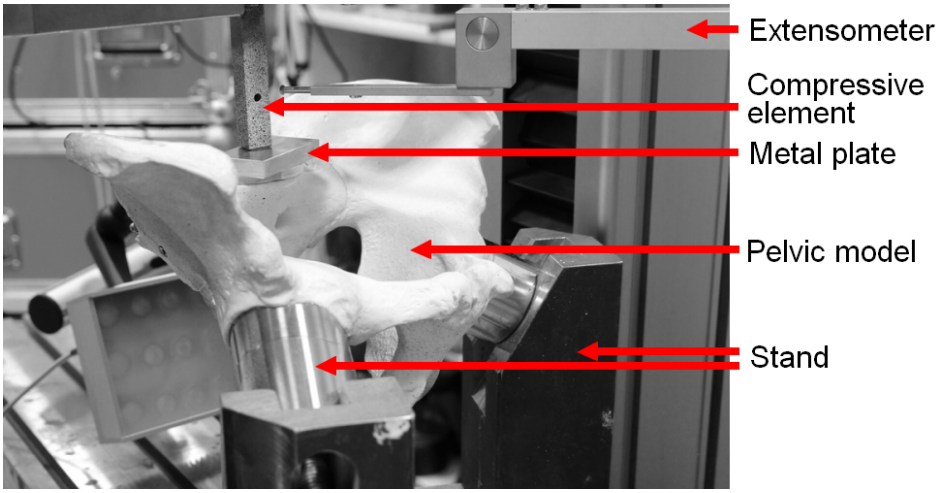

Fig. 2.3: Pelvic model mounted on the stand and placed in the material testing machine. On the top of the sacral base there is a metal plate. In the upper part the compressive element and the extensometer are located. The extensometer is not attached to the compressive element in the captured scene.

2.2.2 Performed measurements

Intact model

As mentioned above, a separate pelvic model was used for testing of all fixation techniques except one. Even though all the models were supposed to be identical, slight differences were recognizable on their surfaces. To reveal the potential diversity in the initial conditions caused either by different material properties of the models or by the mounting on the stand (which could induce a prestress), each model was in the first place tested in the intact state, without any fracture or fixation.

Preliminary tests revealed that the macroscopic damage of the intact pelvic model did not occur for the applied load lower than 600 N. Considering this information, the intact models in this study were loaded to 300 N so as to minimise the risk of damage to the model.

Both the loading and unloading was realised quasistatically, with the speed set to 2.5 N/s. The process was repeated ten times. The results obtained for the intact model were taken into account when the stability of the corresponding fixation technique was discussed.

Fractured and stabilised model

When the measurements of the particular pelvic model were finished, the unilateral transforaminal sacral fracture was artificially created by an orthopaedic surgeon and the given fixation technique was applied. In the following, this state is referred to as the stabilised state. Similarly to the above described experimental measurements, each stabilised model was subjected to ten loading cycles with the loading speed 2.5 N/s. In this case the magnitude of maximal applied force was equal to 500 N, which approximately corresponds to the weight of upper body which the pelvis is bearing at 80 kg human.

Fractured, not stabilised model

One pelvic model with a fracture artificially created was subjected to testing without any fixation device applied. In the following, this state is referred to as the fractured state. Data from this measurement were utilised for the validation of the computational model presented in Chapter 3. This pelvic model was subjected to experimental measurements

identical in all aspects to those performed on the intact models. The loading speed was 2.5 N/mm, the maximal load was equal to 300 N and the loading cycle was repeated ten times.

In comparison to the fractured and stabilised model, the magnitude of maximal applied load was lower as the mechanical strength of the model was significantly reduced after fracturing and excessive loading could cause damage to the material. The maximal applied load was set to 300 N

2.3 Data Acquisition and Processing

The course of the measurement was recorded by two systems. The first group of data was obtained from the materials testing machine, the second from the multi-camera DIC system.

2.3.1 Digital image correlation

The term DIC generally refers to a group of non-contact methods used for obtaining full-field information on strains and displacements from images acquired during experimental measurements [24, 25]. A great advantage of these methods is that they do not affect the course of the measurement and the obtained results as no device is attached directly to the measured object.

Briefly, the process consists of acquisition of 2D images of studied object, followed by image recognition and correlation and the spatial reconstruction of the object. Generally, when three dimensional object is studied, several cameras are used for capturing the object simultaneously from different angles, which is necessary for the subsequent spatial reconstruction.

The cameras have to be calibrated – their mutual positioning and internal camera parameters must be determined. A calibration target, usually with chessboard pattern or regular dot grid with known dimensions, is used for this purpose. The calibration is commonly performed prior to the experimental measurement itself. The scene is calibrated based on the positions of the identifying points (e. g. corners of the squares) in the images from the individual cameras. The process of camera calibration and subsequent scene reconstruction for multiple cameras is described below.

When the linear mapping between camera and real world is assumed, the Direct Linear Transformation (DLT) method [26] can be utilised for the calibration. Its principle for arbitrary number of cameras is explained below. For the description of location of points, homogeneous coordinates are used [26]. They are generated from the inhomogeneous by adding one extra coordinate representing the scale. Thus, the homogeneous coordinates $[X, Y, Z, 1]$ and $k[X, Y, Z, 1] = [kX, kY, kZ, k]$ refer to the same point in the three dimensional space as they differ only by a common non-zero multiple k.

It is assumed that there are n points on the calibration target and the scene is captured by m cameras. The index $i = 1, 2, \ldots, n$ refers to the number of point, the index $j = 1, 2, \ldots, m$ refers to the number of camera.

Homogeneous coordinates of i-th point of the calibration target in the world coordinate system are $\mathbf{X}_i = [X_i, Y_i, Z_i, W_i]^T$. In the image acquired by the j-th camera, the i-th point is represented by homogeneous coordinates $\mathbf{x}_{ji} = [x_{ji}, y_{ji}, w_{ji}]^T$ in the image coordinate system of the j-th camera. When there is a sufficient number of point correspondences $\mathbf{X}_i \leftrightarrow \mathbf{x}_{ji}$, camera matrices $\mathbf{P}_j$ can be computed for each camera.

The camera matrix P_j can be computed using equation

$$\mathbf{x}_{ji} = \mathbf{P}_j \mathbf{X}_i. \tag{2.1}$$

Multiplication by $\mathbf{x}_{ji}$ leads to form

$$\mathbf{0} = \mathbf{x}_{ji} \times \mathbf{P}_j \mathbf{X}_i. \tag{2.2}$$

The matrix $\mathbf{P}_j$, which is a 3×4 matrix, can be rewritten into a 12×1 vector $\mathbf{p}_j$

$$\mathbf{p}_j = \begin{bmatrix} \mathbf{p}_{j1}^T \\ \mathbf{p}_{j2}^T \\ \mathbf{p}_{j3}^T \end{bmatrix}, \tag{2.3}$$

where $\mathbf{p}_{jk}$, $k = 1, 2, 3$, is the k-th row of the P_j matrix.

The eq. (2.2) can be rewritten as

$$\begin{bmatrix} \mathbf{0}^T & -w_{ji}\mathbf{X}_i^T & y_{ji}\mathbf{X}_i^T \\ w_{ji}\mathbf{X}_i^T & \mathbf{0^T} & -x_{ji}\mathbf{X}_i^T \\ -y_{ji}\mathbf{X}_i^T & x_{ji}\mathbf{X}_i^T & \mathbf{0}^T \end{bmatrix} \begin{bmatrix} \mathbf{p}_{j1}^T \\ \mathbf{p}_{j2}^T \\ \mathbf{p}_{j3}^T \end{bmatrix} = \mathbf{0}. \tag{2.4}$$

As these three equations are linearly dependent, only the first and the second are used

$$\underbrace{\begin{bmatrix} \mathbf{0}^T & -w_{ji}\mathbf{X}_i^T & y_{ji}\mathbf{X}_i^T \\ w_{ji}\mathbf{X}_i^T & \mathbf{0^T} & -x_{ji}\mathbf{X}_i^T \end{bmatrix}}_{\mathbf{A}_{ji}} \underbrace{\begin{bmatrix} \mathbf{p}_{j1}^T \\ \mathbf{p}_{j2}^T \\ \mathbf{p}_{j3}^T \end{bmatrix}}_{\mathbf{p}_j} = \mathbf{0}. \tag{2.5}$$

The size of the $\mathbf{A}_{ji}$ matrix is 2×12. For the set of n points, the matrix $\mathbf{A}_j$ with size $2n \times 12$ is obtained

$$\mathbf{A}_j = \begin{bmatrix} \mathbf{A}_{j1} \\ \mathbf{A}_{j2} \\ \vdots \\ \mathbf{A}_{jn}. \end{bmatrix}. \tag{2.6}$$

Using this form, a set of equations

$$\mathbf{A}_j\mathbf{p}_j = \mathbf{0} \tag{2.7}$$

is solved for each camera.

As the real digital images contain noise and the accuracy of mapping is limited by the camera resolution, the set of equations (2.7) does not have the exact solution; therefore, an approximate solution of $\mathbf{p}$ is found by minimising $||\mathbf{A}_j\mathbf{p}_j||$ [26].

When the matrices $\mathbf{P}_j$ are determined, the spatial coordinates of any point $\widehat{\mathbf{X}}$ can be determined based on its image coordinates $\widehat{\mathbf{x}}_j = [\widehat{x}_j, \widehat{y}_j, \widehat{w}_j]^T$ in all cameras. Following equation must be satisfied for each camera

$$\mathbf{0} = \widehat{\mathbf{x}}_j \times \mathbf{P}_j\widehat{\mathbf{X}}. \tag{2.8}$$

The set of equation which has to be solved to get the spatial coordinates $\widehat{\mathbf{X}}$ can be written in form

$$\underbrace{\begin{bmatrix} \widehat{y}_1\mathbf{p}_{13} - \widehat{w}_1\mathbf{p}_{12} \\ \widehat{w}_1\mathbf{p}_{11} - \widehat{x}_1\mathbf{p}_{13} \\ \widehat{y}_2\mathbf{p}_{23} - \widehat{w}_2\mathbf{p}_{22} \\ \widehat{w}_2\mathbf{p}_{21} - \widehat{x}_2\mathbf{p}_{23} \\ \vdots \\ \widehat{y}_m\mathbf{p}_{m3} - \widehat{w}_m\mathbf{p}_{m2} \\ \widehat{w}_m\mathbf{p}_{m1} - \widehat{x}_m\mathbf{p}_{m3} \end{bmatrix}}_{\mathbf{B}} \widehat{\mathbf{X}} = \mathbf{0}, \tag{2.9}$$

where the size of the $\mathbf{B}$ matrix is $2m \times 4$.

During calibration and the subsequent spatial reconstruction, the points in the individual images can be matched either manually or by using an automatic algorithm. If the aim is to get a reconstruction of the whole surface of the studied object, the surface has to be covered by some stochastic pattern, either given by the nature of the object or applied manually. In case of experimental study presented in this thesis, random black and white pattern was sprayed on the studied surface of the solid-foam pelvic model. This pattern allows the DIC algorithm to analyse the images and match them automatically.

During the measurements presented in this study, commercial software package ISTRA 4D was used for the DIC analysis [27]. The DIC system consisted of four monochrome digital cameras and two sources of LED light connected to computer (see Fig. 2.4). The cameras were mounted on one mounting bar and each of them captured the dorsal surface of sacrum from different angle. This adjustment allowed to obtain a three-dimensional reconstruction of the whole captured surface, including the information on displacements and deformations in arbitrary area.

The cameras were capturing images with resolution 4 Mpx and they operated with the frame frequency 0.1 Hz. With reference to the loading speed, a new image was acquired when the force increased/decreased by 25 N.

2.3.2 Material testing machine

The second group of data was obtained from the material testing machine. The data were recorded at frequency 100 Hz and the information on each step contained time, applied

force and displacement of the compressive element measured by an extensometer attached to it.

The two systems – the material testing machine and the DIC system – were synchronised using a TTL signal sent from the DIC software to the testing machine when the image acquisition started. The synchronisation allowed to assign the magnitude of loading force measured by the testing machine to individual images acquired by the DIC system.

2.4 Data Evaluation

When the efficiency of studied fixation techniques was discussed, two evaluation criteria were considered. Firstly it was the stiffness of the stabilised model, and secondly it was the relative displacement of the fractured bone parts.

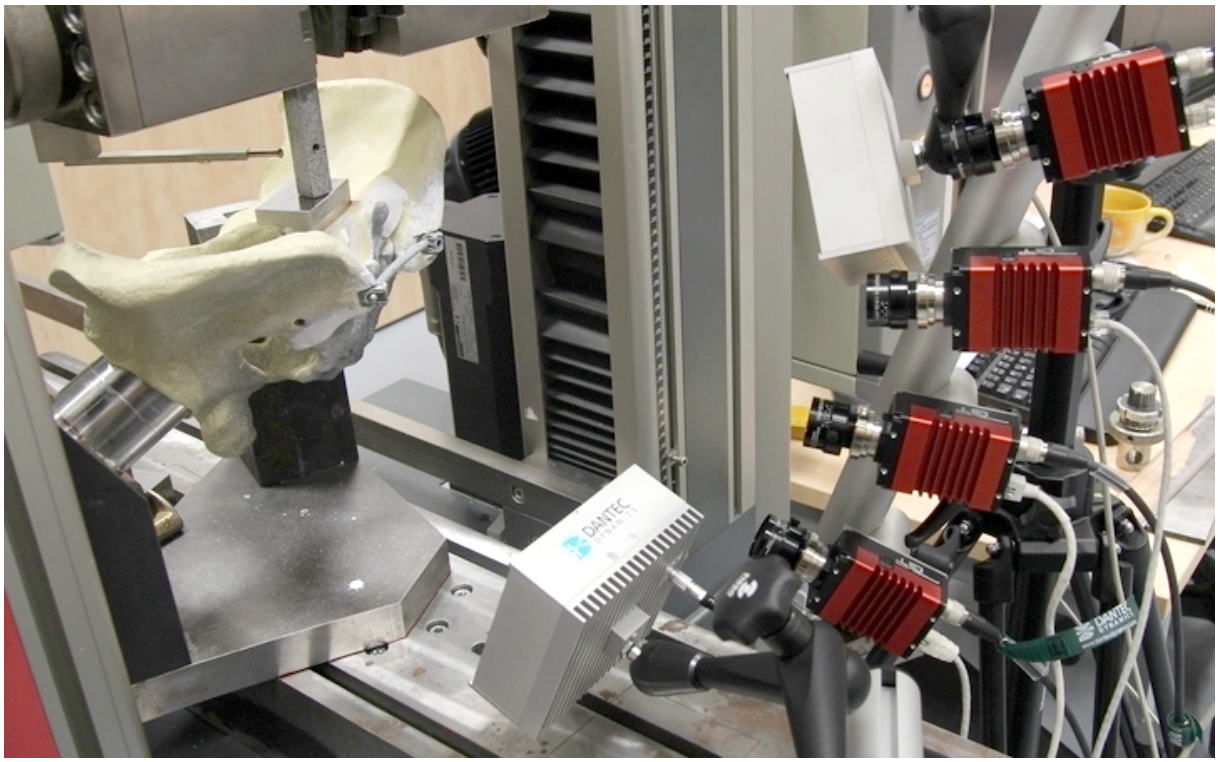

Fig. 2.4: Experimental setup. The cameras on the mounting bar and the lights are displayed in the right part of the picture.

2.4.1 Stiffness of the model

The biomechanical stability of sacral bone fixation technique was evaluated based on the stiffness provided to the fractured bone.

The first method of the stiffness value determination evaluated the vertical displacement of the sacral base. Data from the material testing machine were used for this purpose, as the displacement of sacral base was considered to be identical to that of the compressive element. The stiffness of the solid-foam model in both the intact and the stabilised state was computed using the force-displacement curve obtained from the materials testing machine. The linear part of the curve was approximated by a straight line using the least squares method. The stiffness of the model was assessed as the tangent of this curve.

The principal evaluation parameter was the ratio R^B of the stiffness of the fractured and stabilised model S_F^B and the stiffness of the intact model S_I^B:

$$R^B = \frac{S_F^B}{S_I^B}, \tag{2.10}$$

where the right superscript B refers to base of sacrum, and the right subscripts I and F refer to the intact and fractured state respectively.

2.4.2 Relative displacement of the fractured bone parts

Another important information on behaviour of the fixation technique is the change in the fracture line in consequence of the applied load.

The evaluation criterion was the relative displacement of six pairs of points located along the fracture line. The points, labelled as L1-L6 and R1-R6 are marked in Fig. 2.5. The pairs L1-R1 and L2-R2 were located in the level of S2 vertebra, L3-R3 and L4-R4 in the level of S3, and L5-R5 and L6-R6 in the level of S4. The displacement was evaluated using the data from the DIC system, where the position of each point during loading was recorded.

An additional information was gathered from a three-dimensional reconstruction of the dorsal sacral surface covered by displacement map. This map enabled quick and simple analysis of response of the fractured bone on loading.

Possible movements of the fractured bone parts are illustrated in Fig. 2.6. The behaviour of the fractured bone and the level of significance of particular movement is influenced by the type of the applied fixation technique. Possible movements are the following:

- displacement of both the loaded and the unloaded part in craniocaudal direction (vertical displacement in direction from head to foot), see Fig. 2.6a,
- abduction of the unloaded and adduction of the loaded bone part in the frontal plane (rotation away from the fracture line) which results in the distraction (widening) of the fracture line in the craniocaudal direction, see Fig. 2.6a,
- flexion of the loaded part in the sagittal plane (displacement/rotation of the coccyx to the front), see Fig. 2.6b.

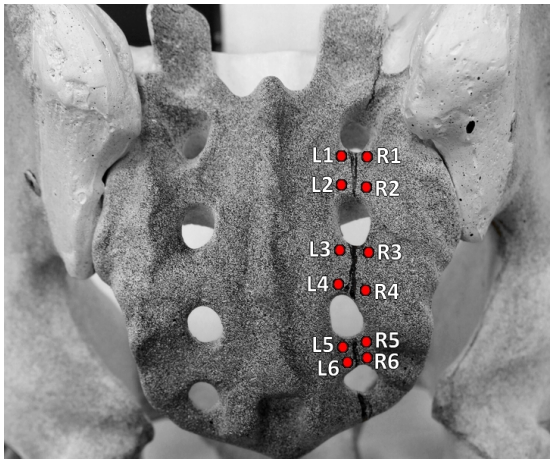

Fig. 2.5: Location of L and R points.

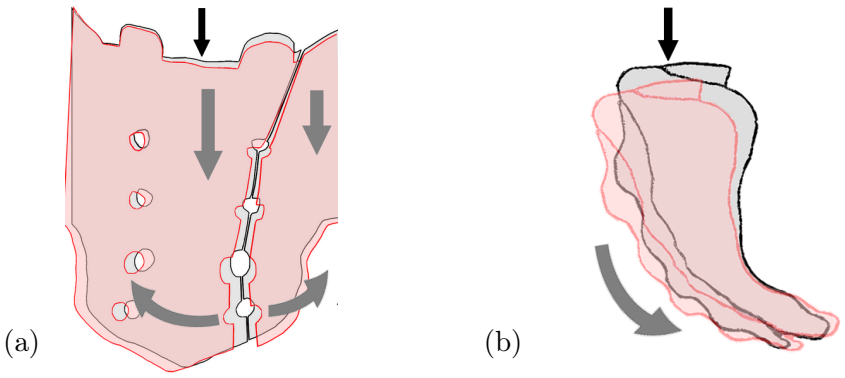

Fig. 2.6: Types of fractured bone parts behaviour under load. The direction of applied load is indicated by black arrow, the possible displacements and rotations by grey arrows.

Experimental and Finite Element Study of Intact and Fractured Pelvic Model

3

One of the aims of this thesis was a preparation and validation of finite element (FE) model of intact and fractured pelvis. The experimental data for the validation were obtained from experimental measurements of solid-foam pelvic model. The measurements were performed on the model in the intact state and in the fractured state, without any surgical reduction performed and without any fixation device applied.

3.1 Experimental Study on Intact and Fractured Model

The material properties of the solid-foam pelvic model were determined by the material testing described in Section 2.1.1:

- Young's modulus $E = 194$ MPa,
- Poisson's ratio $\nu = 0.2$.

Tab. 3.1: Results of the experimental measurements of the intact and fractured model.

Measured parameter	Intact model	Fractured model
Stiffness [N/mm]	$S_I^B = 553$	$S_F^B = 240$
Sacral base vertical displacement at F=300 N [mm]	$u_I^B = 0.578$	$u_F^B = 1.528$
C point total displacement at F=275 N [mm]	$u_I^C = 0.516$	$u_F^C = 1.566$

The study on intact and fractured model yielded the results presented in Tab. 3.1. Values of the stiffnesses S_I^B and S_F^B (see Section 2.4.1) were established as the tangent of the linear approximation of force-displacement curve obtained from data from the material testing machine. Detailed description is provided in Section 2.4. Under the maximum load ($F = 300$ N), vertical displacements u_I^B and u_F^B were determined. These values were assessed from the force-displacement curve obtained from the testing machine; the displacement of the sacral base was considered to be equal to the displacement of the compressive element.

The stiffness ratio R^B (See eq. (2.10)) equals R^B=0.424, which means that the stiffness of the fractured model decreased to 42.4 % of its original value in the intact state. The vertical displacement of sacral base was 2.64 times higher in comparison to the intact bone.

These data were used for the validation of the FE model, together with the displacement map obtained from the DIC system. The map of the intact model under maximal captured load is displayed in Fig. 3.1; the displacement map of the fractured model is shown in Fig. 3.2.

In the intact state, the largest displacement of the dorsal sacrum is measured at the upper tubercles of the median sacral crest. This suggests that the dominant movement of the bone is its rotation in the sagittal plane (See Fig. 2.6b).

During loading of the fractured model, a contact occurred between the fracture sides at the level of S1 vertebra. Therefore, the applied load resulted in displacement of both the loaded and unloaded part which is obvious from the displacement map in Fig. 3.2. The displacement map also suggests that the loaded part both moves vertically and rotates in the frontal plane.

3.2 Finite Element Model

The FE problem was solved in the software for finite element analysis Abaqus [32]. All the parameters for the simulation – geometry, material, boundary conditions and applied load – were set based on the experimental measurements described in Section 3.1 and their setup.

The experiment was designed so that the FE model can be solved using the linear elastostatic. The experimental measurements satisfied following fundamental assumptions

– sufficiently small displacements and deformations, homogeneous and isotropic material, quasistatic loading.

The linear elastic problem is described by 15 equations [31]:

- 3 equilibrium equations

$$\sigma_{ij,j} + f_i = 0, \tag{3.1}$$

- 6 geometric equations

$$\epsilon_{ij} = \frac{1}{2}(U_{i,j} + U_{j,i}), \tag{3.2}$$

- 6 constitutive equations (generalised Hooke's law)

$$\sigma_{ij} = \lambda \epsilon_{kk} \delta_{ij} + 2\mu\epsilon_{ij}, \tag{3.3}$$

where $i, j, k = 1, 2, 3$, σ is the Cauchy stress tensor, f is a body force per unit volume, ϵ is the strain tensor, U is the displacement vector, λ and μ are the Lamé coefficients and δ is the Kronecker delta.

3.2.1 Problem definition

As mentioned above, the problem was solved as linear elastic. The material of the solid-foam pelvic model was considered to be homogeneous and isotropic; therefore, linear

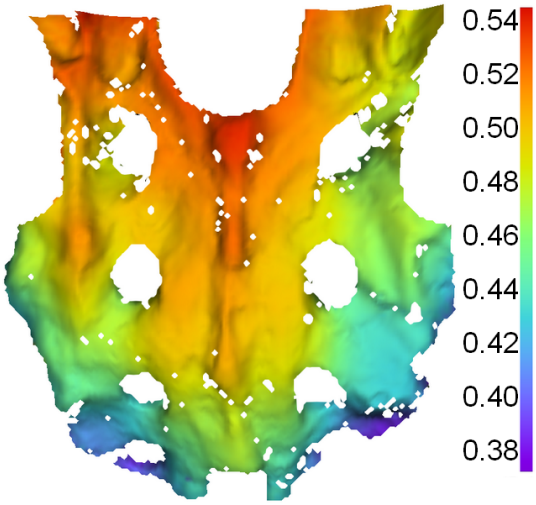

Fig. 3.1: Displacement map of the intact pelvis. Data from the DIC system.

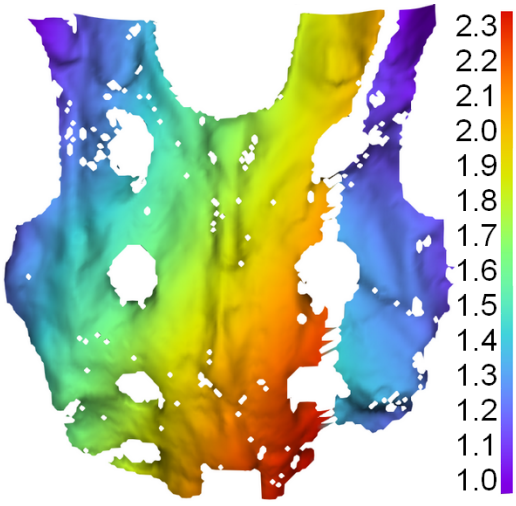

Fig. 3.2: Displacement map of the fractured pelvis. Data from the DIC system.

elastic isotropic material model was considered, with the material parameters presented in Section 3.1.

Coordinate system

So as to easily specify the direction in which the load was to be applied, a local rectangular coordinate system was defined in the model. The xy plane of this coordinate system was set identical to the plane of sacral base while the desired z axis was perpendicular to it. In the z direction, the load was applied and consequently the vertical displacements were evaluated.

Boundary conditions

The static load of 300 N was represented as a concentrated force distributed to all nodes on the sacral base, similarly to the experimental measurement where the load distribution was ensured by the use of the metal plate (see Fig. 3.4). The load was applied perpendicularly to the sacral base. The applied load is illustrated by vertical red arrows in Fig. 3.3.

As displayed in Fig. 3.4, the solid-foam model was rigidly mounted on the stand during experiments which disabled movements and rotations in the acetabula. All nodes in these areas at the FE model were fixed in all directions (see blue markers in Fig. 3.5).

Contact problem

In the analysis of the fractured model, a contact was defined between corresponding surfaces of the fracture sides to prevent their penetration. Selected type of interaction was the standard surface-to-surface contact with a finite sliding formulation [33]. The contact interaction properties involved a non-zero friction coefficient.

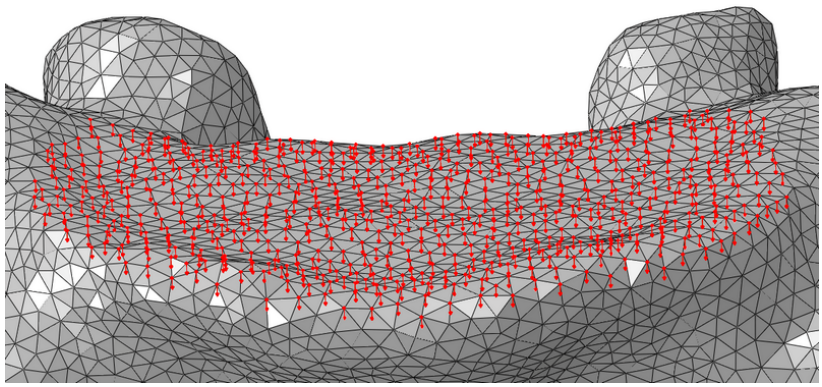

Fig. 3.3: Detailed view of load applied at the sacral base.

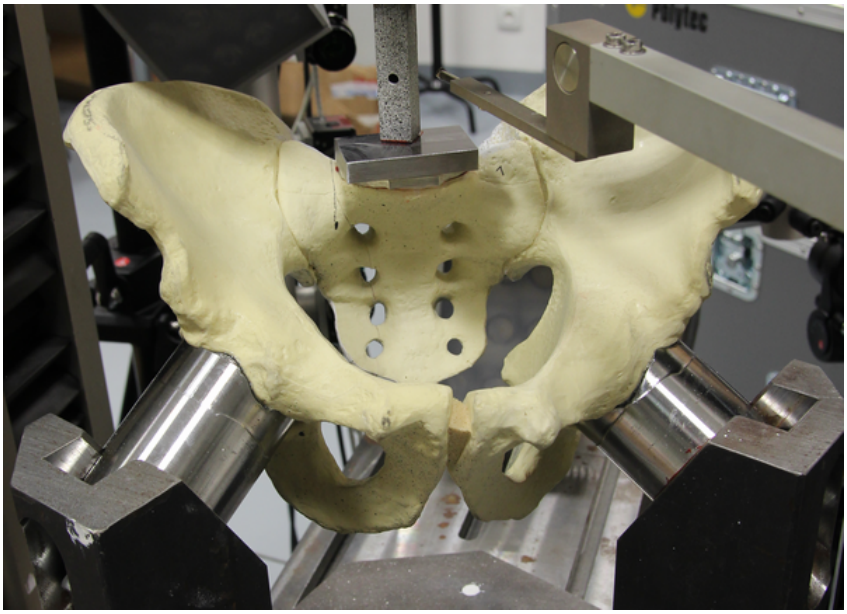

Fig. 3.4: Experimental setup. Pelvic model was fixed in acetabula and loaded at the sacral base.

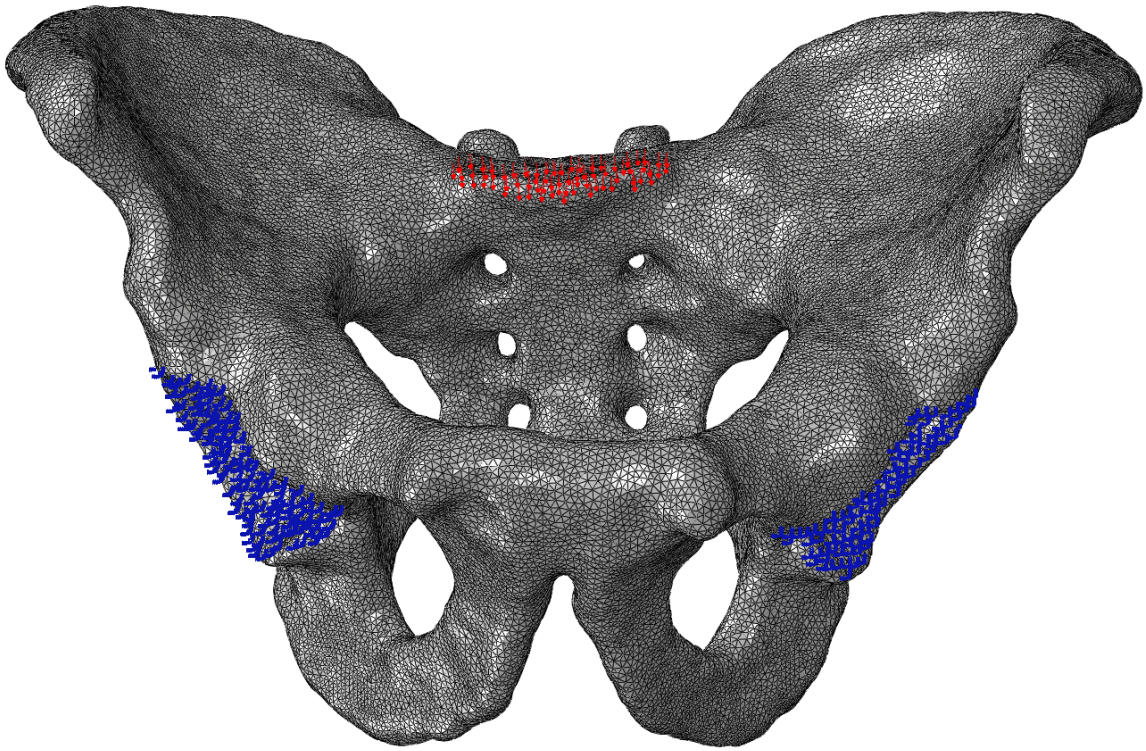

Fig. 3.5: Boundary conditions of the FE model. Blue markers located in acetabula refer to fixed nodes. Red arrows at the sacral base denote the nodes in which the prescribed load was applied.

3.2.2 Finite element pelvic model

The preparation of the FE pelvic model consisted of subtasks common for both intact and fractured models – definition of geometry and mesh. One additional step for fractured pelvis was the modification of the mesh by creating the transforaminal sacral fracture. All of these are described below.

3.2.2.1 Geometry

The computational model was created based on the data obtained from X-ray computed tomography (CT). The CT uses special x-ray equipment – a set of beams sent simultaneously from different angles – to produce cross-sectional image of the scanned object [29, 30]. The object moves through the CT machine so as to obtain a series of images which captures a cross sections of the object in equidistant parallel planes. In medical praxis, the required information can be gathered from the data in the form of separated images, or the pictures may be afterwards put together to produce a 3D model. The principle of this process is illustrated in Fig. 3.6.

The images were processed in the DICOM2FEM software [34]. Using the semiautomatic algorithm, the pixels containing the pelvic model were marked in each image. Consequently, the denoted areas from all images were merged into a discretized 3D object.

The discretized representation of the solid-foam pelvic model was created from the CT scan images with the spatial resolution 21 dpi. The distance between adjacent images

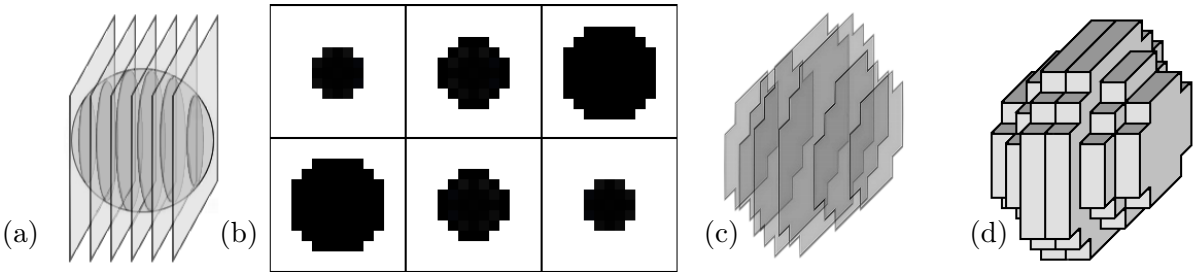

Fig. 3.6: The illustration of the CT scan principle. (a) Parallel planes in which the images of the object were taken, (b) acquired images, (c) images spatially aligned, (d) final 3D model of the scanned object.

was 1.2 mm. The 3D model created by this process is presented in Fig. 3.7a. Selected slices of the pelvic scan are shown in Fig. 3.8.

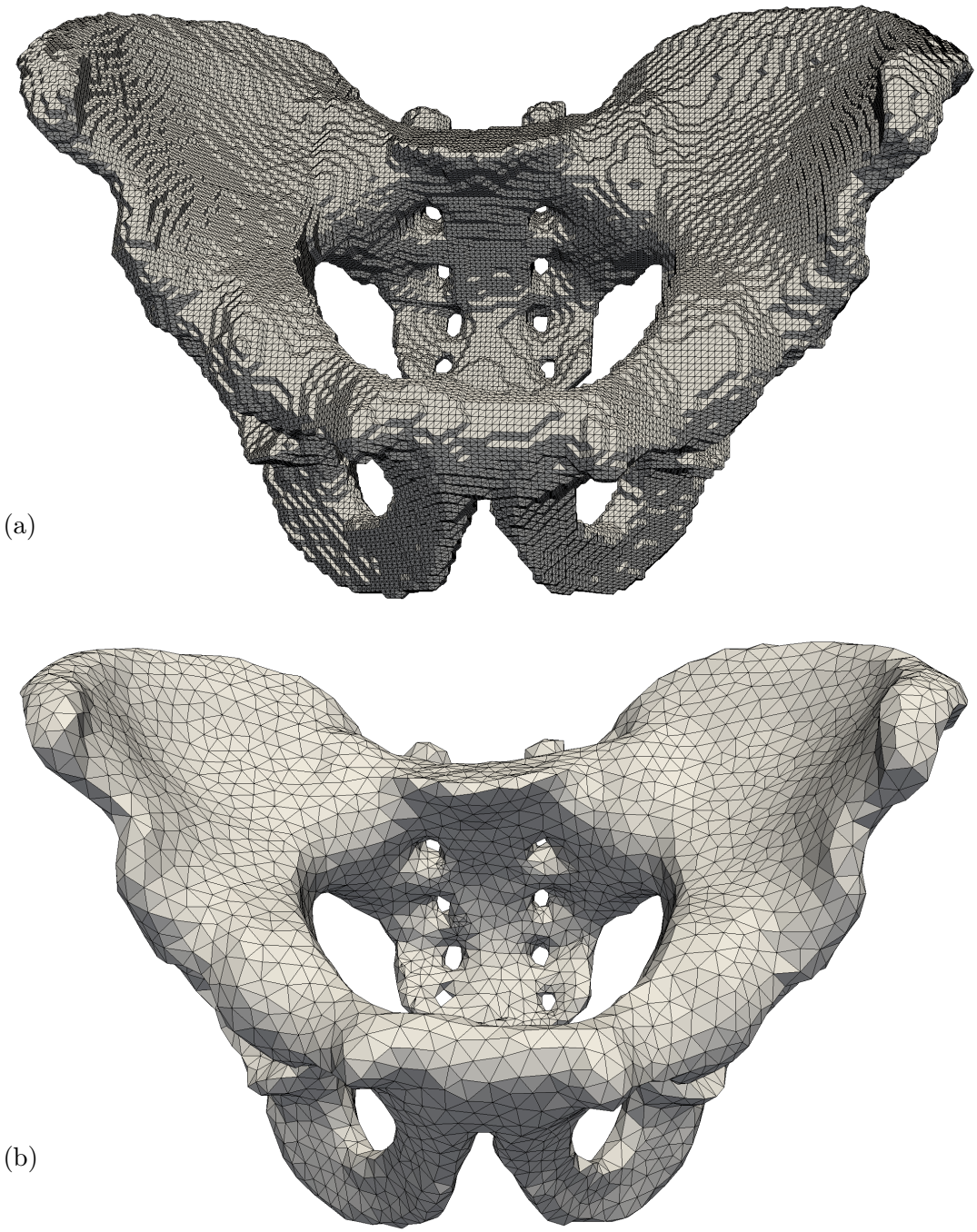

(a)

(b)

Fig. 3.7: Finite element pelvic model. (a) 2D shell object obtained by merging the individual CT images, (b) 3D solid object after smoothing.

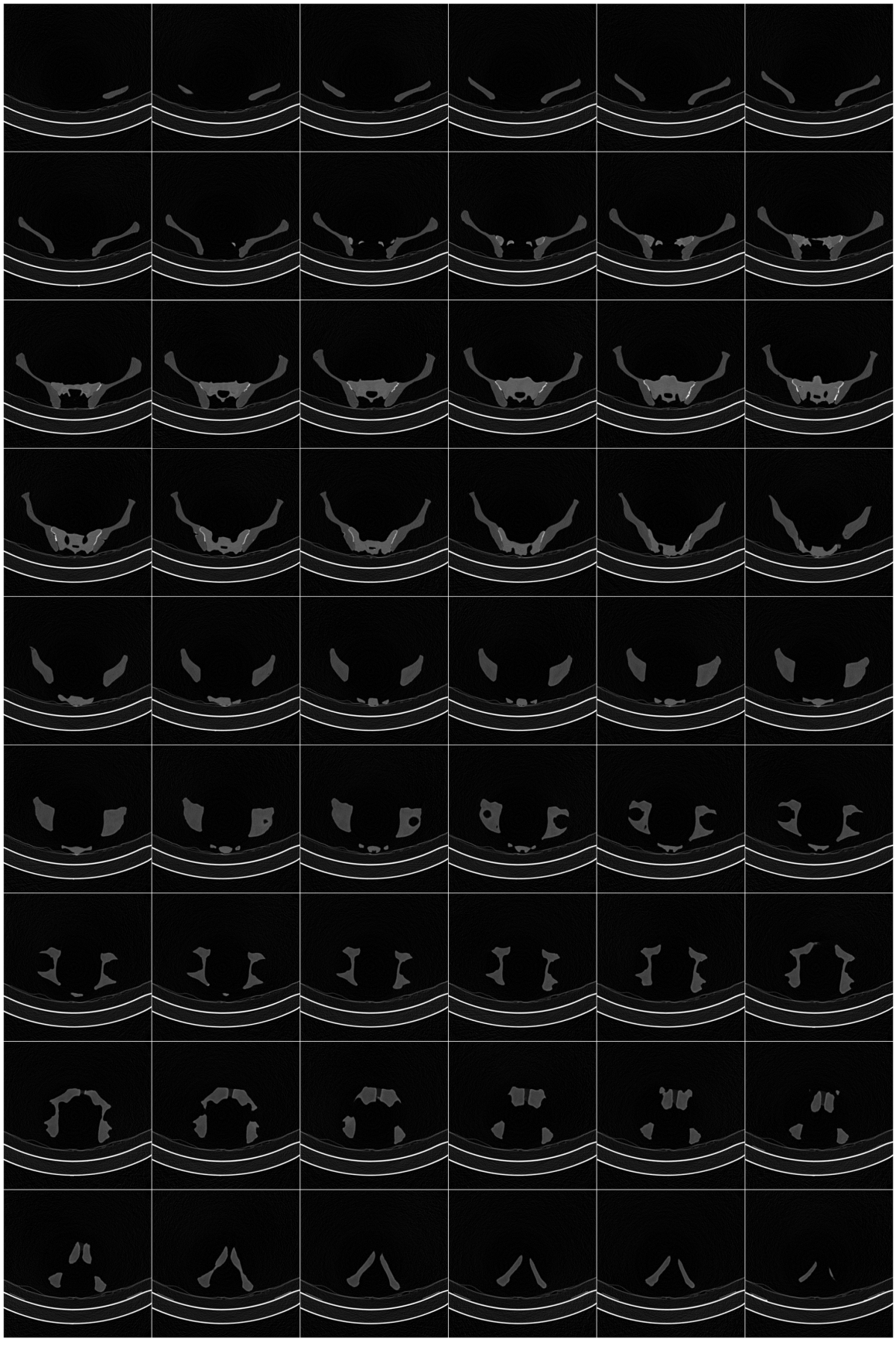

Fig. 3.8: Selected CT scan images of pelvic model.

3.2.2.2 Mesh

The output from the CT scans is a 2D shell, hollow inside, with only the surface being meshed with triangular elements. This object was further modified by DICOM2FEM utilities and by the Gmsh 3D finite element mesh generator [35]. Using these software, the 2D shell was transformed into a 3D solid made of linear tetrahedral elements, smoothed and remeshed according to the element size requirements. Illustration of the smoothed mesh is presented in Fig. 3.7b.

Mesh convergence study

So as to reveal the optimal measure of mesh fineness with respect to required accuracy of obtained results, five meshes with different element size were created. Their parameters – average length of the element edges, number of nodes and number of elements – are described in Tab. 3.2. For these meshes, the mesh convergence study was conducted on the intact model.

In the finite element software Abaqus, the same analysis was performed on each mesh and the displacement of selected point on the sacral base was compared. In Fig. 3.9 the dependence of the displacement on the number of elements is depicted. Based on the slope of the curve, it can be concluded, that the difference in displacement obtained for meshes IV and V is negligible. Therefore, in order to decrease the computational time, the mesh IV was used.

Tab. 3.2: Parameters of the generated meshes

Mesh	Mean edge length [mm]	Number of nodes	Number of elements
I	12.1	1806	5500
II	8.8	4983	17089
II	5.2	20976	86575
IV	2.9	113685	556385
V	1.5	671149	3673699

3.2.2.3 Fracture

The selected mesh type IV was modified so as to prepare the computational model of fractured pelvis. On the plastic pelvic models the transforaminal fracture was artificially created by the orthopaedist.

In the computational model, the mesh was adjusted in the finite element pre-processor HyperMesh [36]. The fracture line was established by two parallel planes placed to each of the five vertebrae. The initial gap between those planes denoting the sides of the fracture was set to 0.02 mm.

The process of fracture creation for one vertebra is displayed in Fig. 3.10. Fig. 3.10a shows the mesh before creating the fracture. The mesh in the area where the fracture line was incident was refined and shape of concerned elements was adjusted so that given edges were aligned with the intersection curve of the pelvis and the two planes determining the fracture (Fig. 3.10b). As a result, a strip of elements was obtained (see the highlighted area in Fig. 3.10b). Subsequently these elements were deleted and fracture with desired gap between the bone parts was created (Fig. 3.10c). The final mesh with the created fracture is presented in Fig. 3.11.

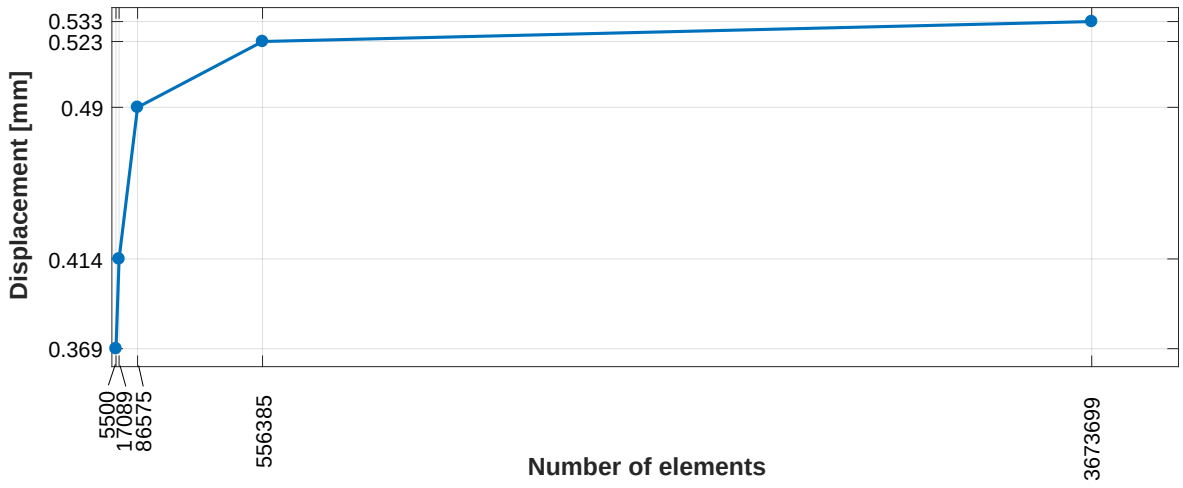

Fig. 3.9: Mesh convergence

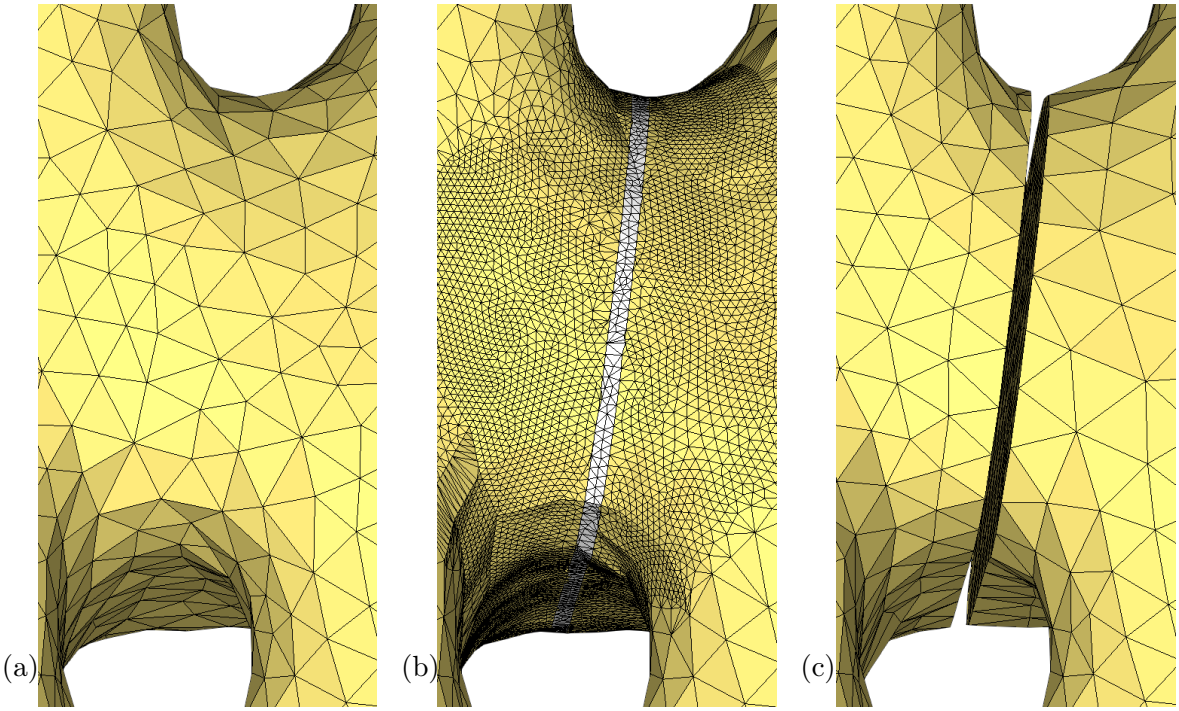

Fig. 3.10: The process of fracture creation in the level of S4 vertebra. (a) Original state, (b) refined mesh with elements to be deleted highlighted, (c) finale state where the fracture is created and the mesh is adapted based on the original element size.

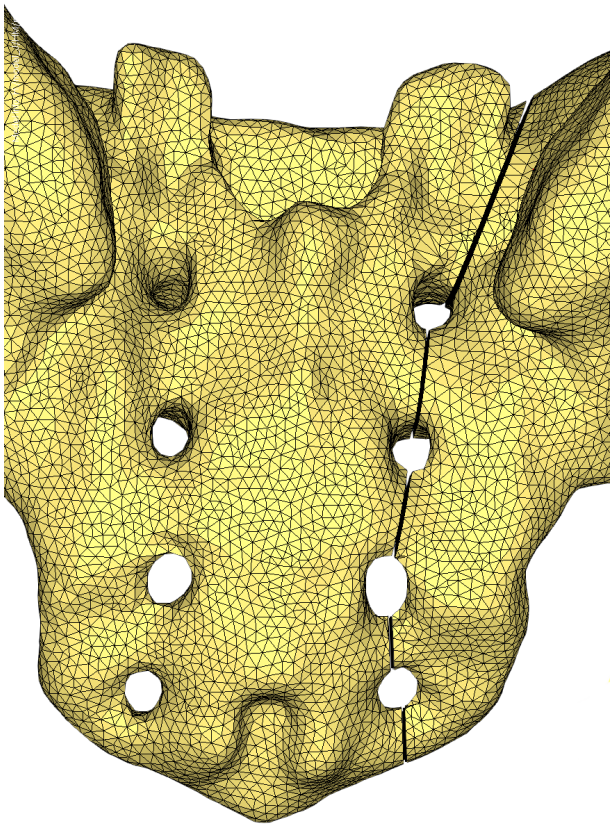

Fig. 3.11: Mesh of the sacral bone with created fracture.

3.2.3 Results of Intact Pelvis

The first tested FE model was the intact pelvis. It was validated based on three criteria, each of them is described below. Corresponding results from the experimental measurements are presented in Tab. 3.1.

Vertical displacement of sacral base and stiffness S_I^B

In the FE model, the vertical displacement of the sacral base was measured in the point at the centre of the sacral base, in place where the compressive element was positioned during the experimental measurement. The displacement was equal to ${}^F u_I^B = 0.523$ mm, where the left superscript refers to FE analysis. In comparison to the experimental measurement, the displacement in the FE model was 10.9 % lower.

Fig. 3.12 presents the force-displacement curves obtained from the experimental measurements and the FE model.

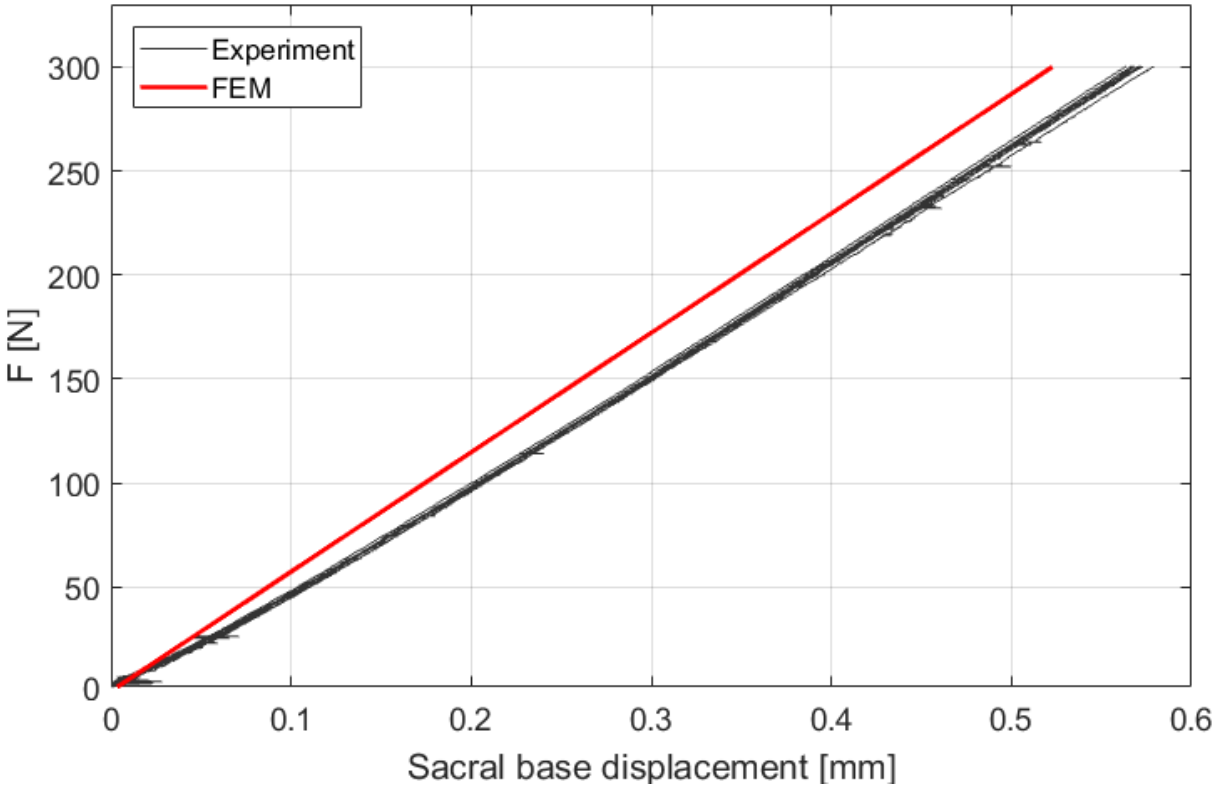

Fig. 3.12: Force-displacement curve of sacral base of intact model. Comparison of experimental and FE model results.

Using the same method as in the experimental analysis, the stiffness of the FE model was determined from the force-displacement curve (the red line in Fig. 3.12). The stiffness value equals ${}^{F}S_{I}^{B} = 574$ N/mm, which is 4 % higher than the value obtained from the experimental measurements.

The difference between FE model and the experiment in the sacral base displacement was most likely caused by the nonlinear behaviour at the beginning of the experimental measurement. When considering only the linear part of the curves, there is no such significant difference in the slope of the curves. This assumption is supported by the values of stiffnesses, where the difference is only 4 %.

Total displacement of point C

Total displacement of the point located at the uppermost tubercle at the median sacral crest, labelled as point C, was evaluated. Under the loading force $F = 275$ N, which was

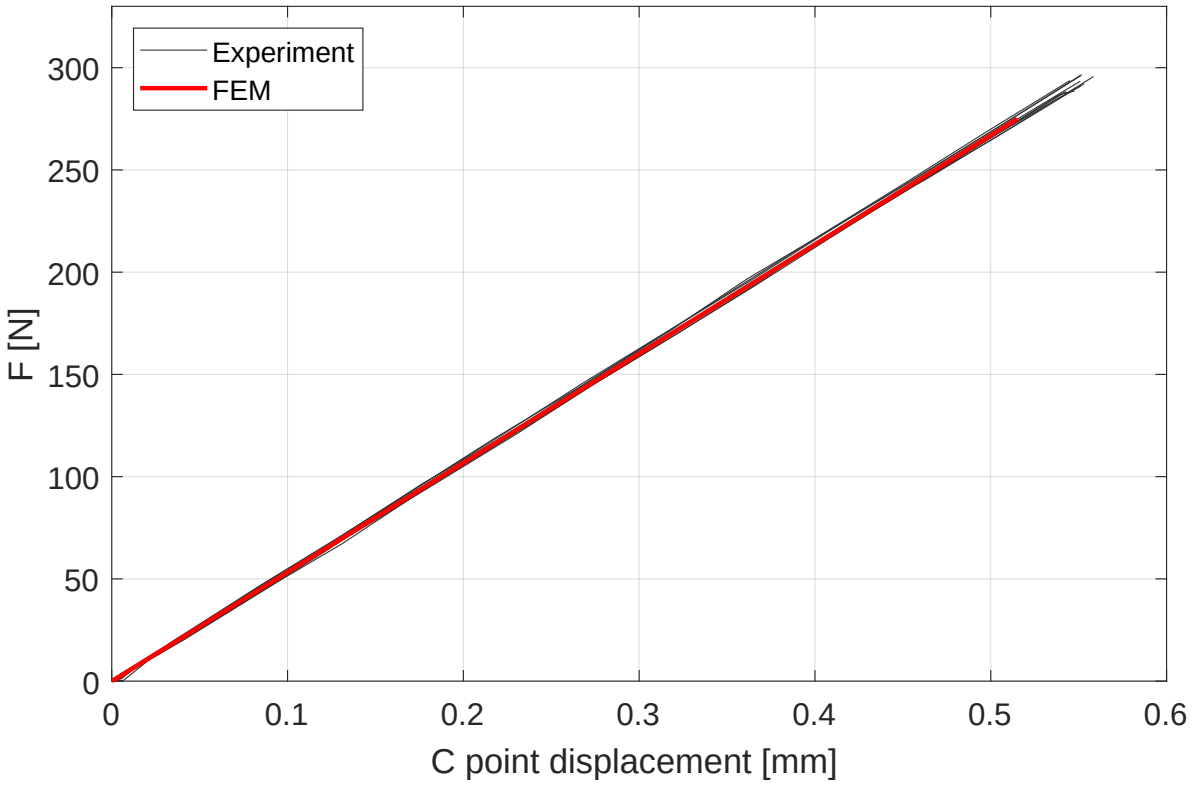

Fig. 3.13: Force-displacement curve of C point of intact model. Comparison of experimental and FE model results.

the force used for the evaluation of the DIC data, the C point displacement was equal to ${}^{F}u_I^C = 0.518$ mm. The value differs from the experimental result (see Tab. 3.1) by 0.4 %.

Fig. 3.13 displays the force-displacement curves of the point C1. It is obvious that the curve obtained from the FE analysis corresponds well to the curves obtained from the DIC system.

Displacement map

The displacement map of the intact model obtained from the FE analysis is displayed in Fig. 3.14a. For the comparison with the experimental measurement, the displacement map obtained from the DIC system is presented in Fig. 3.14b. It can be concluded that the results of the FE analysis correspond well to those of the experiment. As expected, the displacement map is symmetric with respect to the sagittal plane. The largest total displacement of the dorsal surface of sacrum is observed at the uppermost tubercle at the median sacral crest, which suggests the dominant movement of the sacrum was its rotation in the sagittal plane.

Considering all the presented results it can be concluded that the behaviour of the FE model of intact pelvis is in very good agreement with the experimental measurements and the model can be considered as valid.

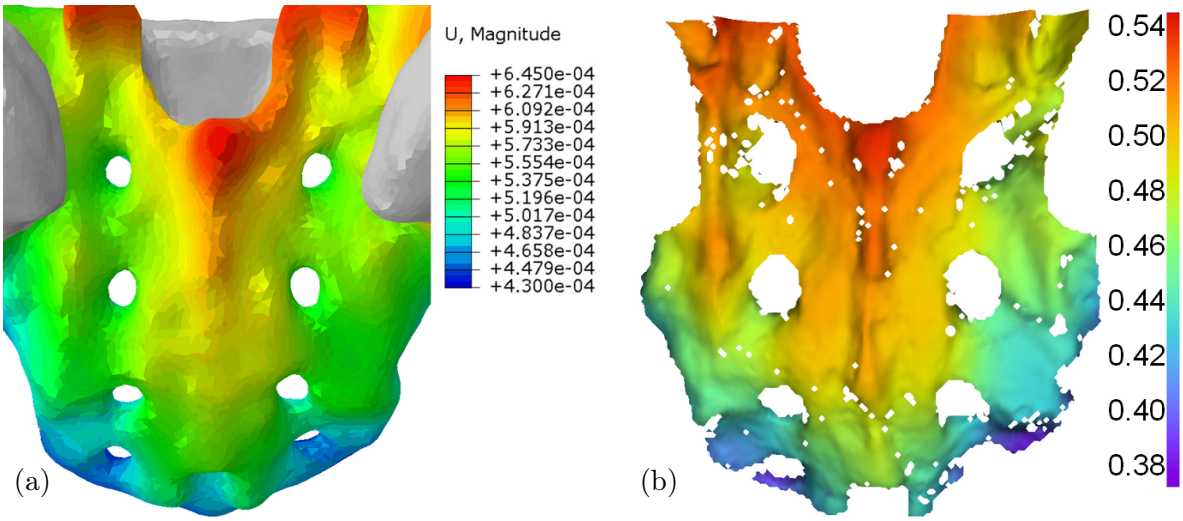

Fig. 3.14: Displacement of the intact model. Comparison of (a) experimental and (b) FE model results.

3.2.4 Results of Fractured Pelvis

The validated FE model of intact pelvis was subsequently modified by creation of a transforaminal sacral fracture. The results obrained from the experimental testing of the solid-foam model in the fractured state (see Tab. 3.1) were used for validation of the fractured FE model.

The contact problem defined at the fractured model required a specification of friction coefficient f. As its value was not investigated yet, the sensitivity analysis of the foam-to-foam friction was performed for five values of f, $f = 0.3, 0.5, 0.8, 1, 1.2$. Fig. 3.15 presents the relation between the friction coefficient and the sacral base displacement. The best agreement with the experimental data was achieved for $f = 0.5$ (8.4 % difference) and $f = 0.8$ (3.9 % difference). The values of stiffness S_F^B for particular friction coefficients are presented in Fig. 3.16. According to this parameter, the most accurate results were obtained for $f = 0.8$ (8.9 % difference between FE and experimental data) and $f = 1$ (3.7 % difference); the stiffness ratio equals ${}^F R^B = 38.1$ % (10.1 % difference) and ${}^F R^B = 43.4$ % (2.3 % difference), respectively.

Considering both the sacral base displacement and the stiffness of the model, the best agreement with the experimental data were achieved with the friction coefficient $f = 0.8$.

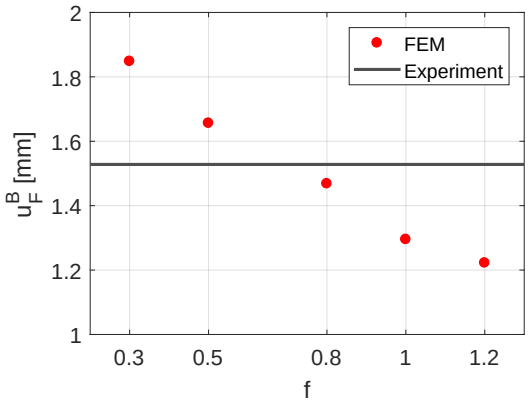

Fig. 3.15: Influence of friction coefficient on the sacral base displacement u_F^B. Grey line denotes the displacement obtained from the experimental measurements, the red dots denote values of sacral base displacement for particular values of the friction coefficient f.

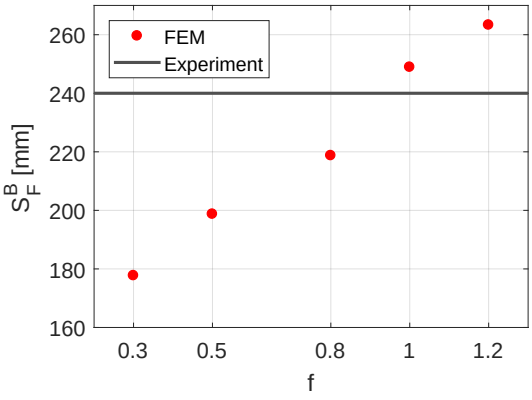

Fig. 3.16: Influence of friction coefficient on the stiffness S_F^B. Grey line denotes the stiffness obtained from the experimental measurements, the red dots denote values of stiffness for particular values of the friction coefficient f.

Displacement map

The FE results of the fractured model presented in Fig. 3.17a are displayed for the model with the friction coefficient $f = 0.8$. The displacement map of fractured pelvis under maximal loading obtained from the DIC system is displayed in Fig. 3.17b. Certain common characteristics of the bone movements can be seen in both images. The displacement of the unloaded part is significantly lower than that of the loaded part of the bone. The largest displacement occurred in both cases along the fracture line at the loaded part, however, the maximal value occurred in the level of S5 vertebra in the experimental measurement while the maximal displacement in the FE model is located in the level of S1 vertebra. This suggests that the more notable movement during the experimental measurement was the adduction of the loaded part. In the FE model, both the adduction of the loaded part and its vertical displacement were significant.

In can be concluded that both the intact and fractured FE models of human pelvis are valid and reliable. Fair agreement – difference lower than 11 % – with the experimental data was achieved in all studied criteria. Further improvement of the FE model could be achieved by modification of the material model to involve the nonlinear behaviour of the solid foam. However, the maximal strain in the FE model was lower than 1 %, which is in the range of linear response of the solid foam.

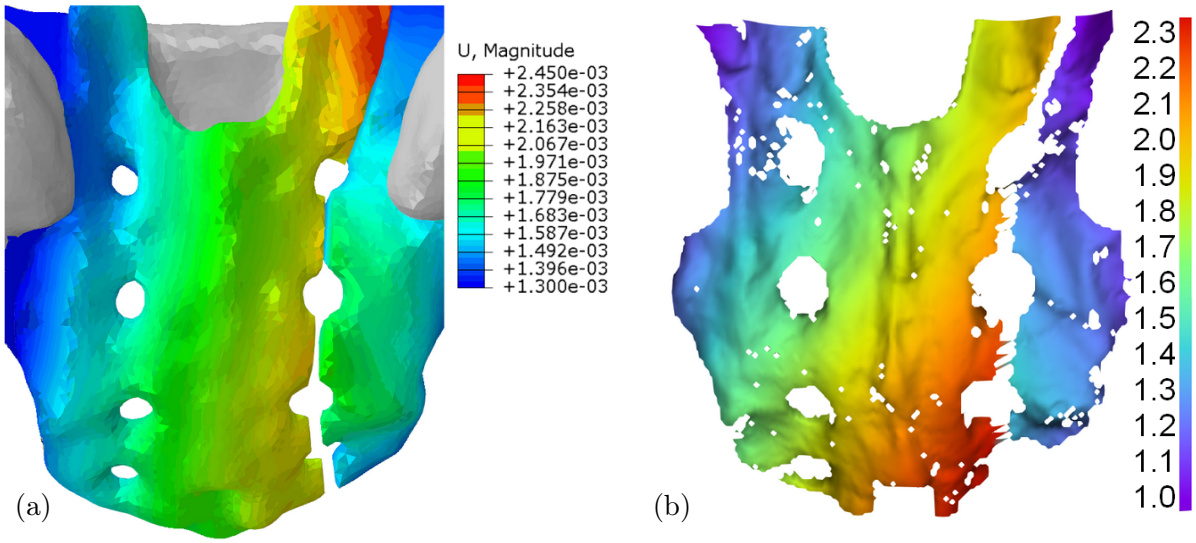

Fig. 3.17: Displacement of the fractured model. Comparison of (a) experimental and (b) FE model results.

Biomechanical Study of Fixation Techniques

4

In this biomechanical study ten fixation techniques utilised for stabilisation of transforaminal sacral fracture were experimentally tested. Their list is provided in Tab. 4.1 together with their labelling which will be used in this chapter. The information on application of these techniques is provided in Section 1.3.3 and Fig. 1.9.

Each fixation technique was studied in terms of its efficiency which was evaluated as the ability to sufficiently restore the mechanical strength of the fractured bone. Except from the overall comparison of all the tested techniques, a study focused on selected groups of fixators are presented in this chapter . The course of each experimental measurement on each pelvic model was recorded and an extensive group of data were obtained and

Tab. 4.1: An overview and labelling of fixation techniques.

Label	Description
TIFI-A	Single TIFI, supraacetabular position
TIFI-C	Single TIFI, classical position
TIFI-D	Dual TIFI
ISS-$\parallel$	Dual ISS, parallel to the sacral base
ISS-$\perp$	Dual ISS, perpendicular to sacral base
TFIS-P	TIFI-A + Single partially threaded ISS
TFIS-F	TIFI-A + Single fully threaded ISS
SB-1	Dual SB, measurement 1
SB-2	Dual SB, measurement 2
TP-S	Single TP
TP-D	Dual TP

analysed. Based on these data, the behaviour and properties of fixation techniques were investigated and compared.

As mentioned is Section 2.2.2, each model in each tested state was subjected to ten loading cycles. After investigation of all the results it was found out that results of the first loading cycle generally differ from the rest as the model had to adapt to the applied load. These first measurements were omitted from the data evaluation.

First set of information was gained from the force-displacement curve recorded by the material testing machine. The linear part of the curve was approximated by a straight line using the least squares method. Stiffness values S_I^B and S_I^F of the model (See Section 2.4) were determined as the tangent of the line.

The interval to be approximated was selected same for all the measurements, considering the shape of all the force-displacement curves. In the study of intact models, the approximated interval was from $F = 150$ N to $F = 300$ N. In the stabilised models study, the interval corresponding to force $F = 250$ N to $F = 500$ N was selected. Loading parts of selected curves are displayed in Fig. 4.1. The area that was approximated is highlighted by thicker red line.

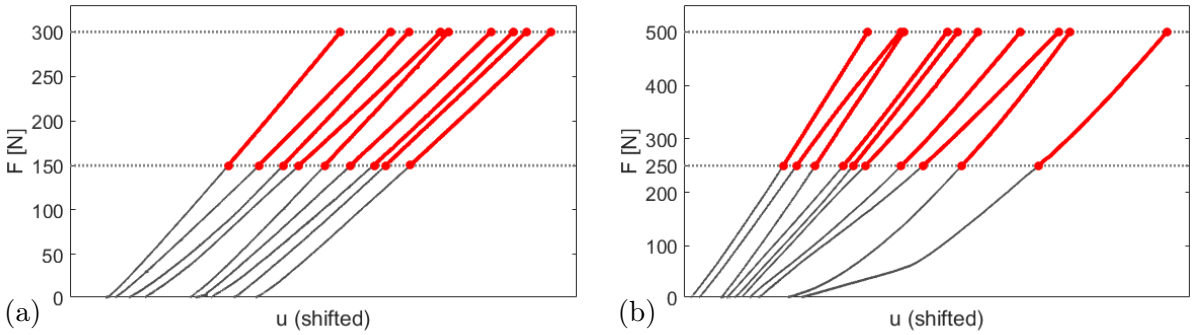

Fig. 4.1: Loading part of the force-displacement curves of selected measurements performed on (a) intact models, (b) fractured models. The data were shifted in horizontal direction for better orientation in the graph.

4.1 Study on transiliac internal fixators

The firstly studied fixation techniques were those involving one or two TIFI. The aim was to reveal the influence of its positioning on its performance. In the first studied case (labelled as TIFI-A, Fig. 1.9a), one TIFI was applied approximately in the level of S1 vertebra; in the second case (TIFI-C, Fig. 1.9b) the TIFI was positioned higher along the iliac crest, approximately in the level of sacral base; in the third case (TIFI-D, Fig. 1.9c), two TIFI were applied in both described positions simultaneously.

The obtained results of stiffness are presented in Tab. 4.2. When evaluating the data it has to be considered that TIFI-C was tested after TIFI-D at the same pelvic model, which means the mechanical properties of the model could have been affected. However, no decrease in the stiffness S_F of TIFI-D was observed. The value remained almost constant during all the evaluated measurements (See Fig. 4.2), which suggests that the model quality was not affected before the testing of TIFI-C.

Tab. 4.2: Stiffness of pelves with TIFI fixation technique.

Technique	S_I^B [N/mm]	S_F^B [N/mm]	R^B
TIFI-A	603	458	0.76
TIFI-C	553	370	0.67
TIFI-D	553	420	0.76

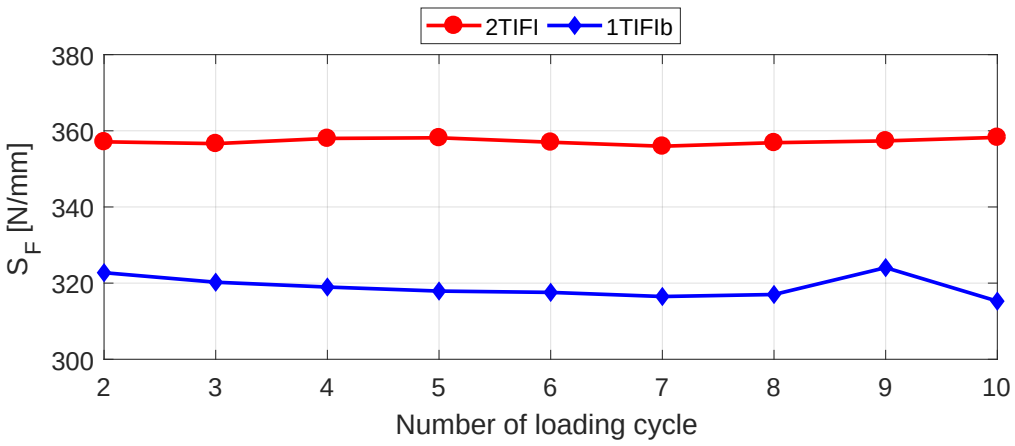

Fig. 4.2: The stiffness S_F of TIFI-D and TIFI-C in the individual loading cycles.

The value of stiffness ratio presented in the last column of Tab. 4.2 is almost identical for TIFI-A and TIFI-D; in both cases the stiffness was restored to 76 % of its initial value (i.e. the stiffness in the intact state). The mechanical strength of pelvis stabilised by TIFI-C was lower; the technique provided the stiffness equal to 67 % of its initial value.

The displacement map of the sacral surface displayed on the three dimensional reconstruction of the pelvic model is shown in Fig. 4.3. Displacement under maximal captured load is presented. Similar behaviour is observed in TIFI-A and TIFI-D, where the movement of the unloaded part is significantly smaller than the movement of the loaded part.

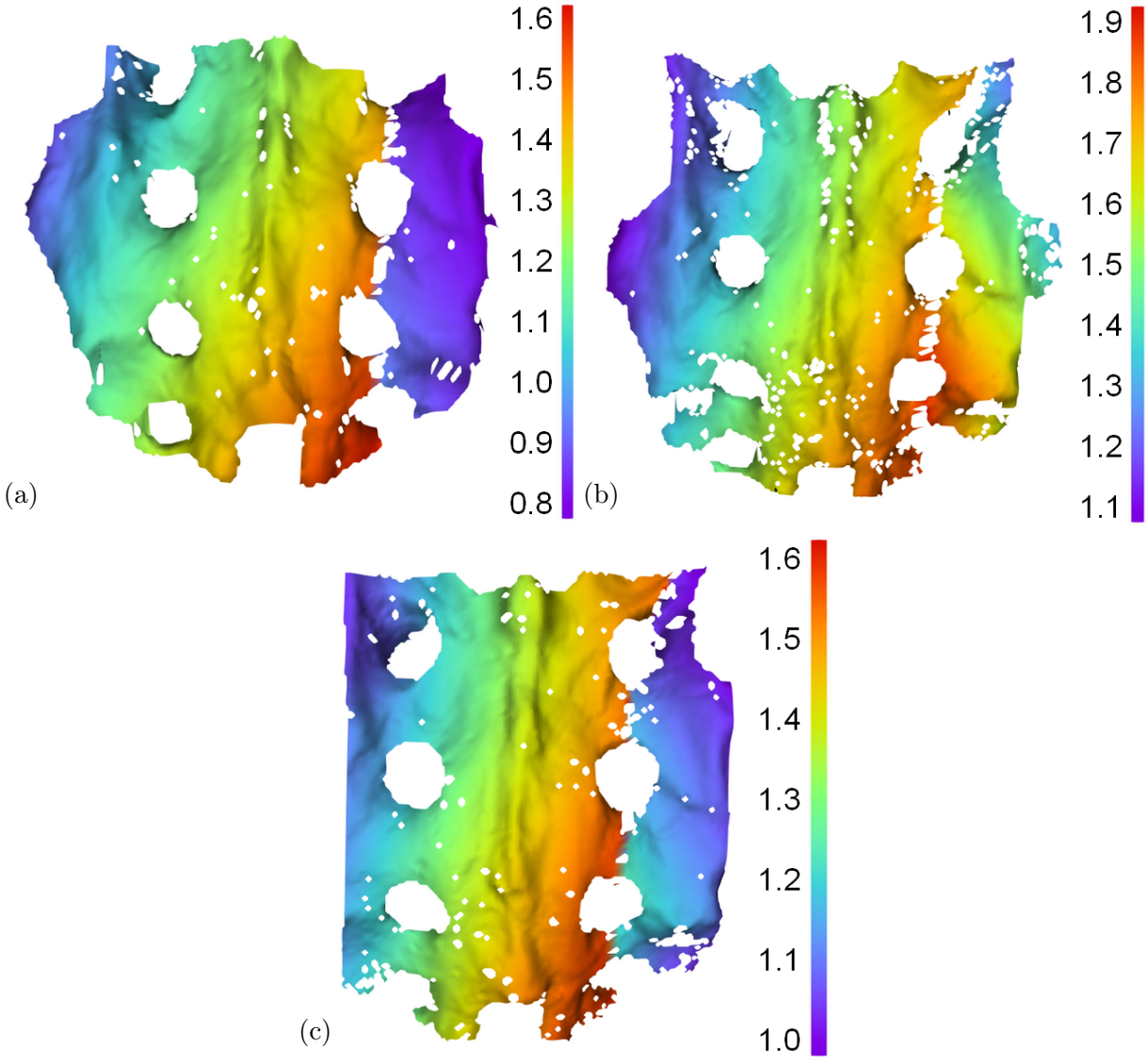

Fig. 4.3: Displacement map of fractured pelvic models stabilised by TIFI. Total displacement in mm is displayed. (a) TIFI-A, (b) TIFI-C, (c) TIFI-D.

This behaviour reveals that the parts of the fractured bone experienced large relative vertical displacement of the bone parts. As can be seen in Fig. 4.4, the relative displacements of the bone parts, expressed in terms of relative displacements of the L-R pairs (see Fig. 2.5), are nearly equal for both techniques.

Contrary to that, TIFI-C exhibits different behaviour. The movement of the unloaded part is not negligible in this case; the nature of the displacement map reveals the adduction of the loaded and abduction on the unloaded part, which leads to the distraction of the fracture line in its lower part. This behaviour is obvious from Fig. 4.4, where the relative displacement of the L-R pairs in level of S3 and s4 vertebrae is significantly larger than at TIFI-A and TIFI-D. This effect was most caused by the fact that the fixator was applied above the level of loading (i.e. the level of sacral base). The lower positioned TIFI did not allow such significant distraction of the fracture line and enabled primarily the vertical displacement of the loaded part.

According to the above described results, there is no significant advantage in the application of two TIFI instead of one from the mechanical point of view as both the TIFI-A and TIFI-D exhibit very similar behaviour. Based on these observations, it is more suitable to apply the fixator in the supraacetabular position, below the level of the sacral base, so as to keep the fracture gap width stable along the whole fracture line.

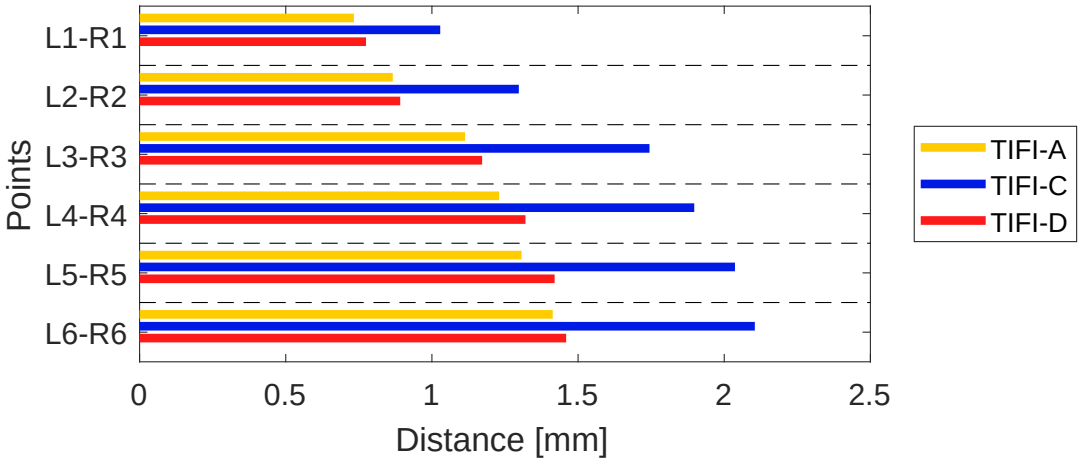

Fig. 4.4: Relative displacement of L-R points for maximal load of models with fracture stabilised by TIFI.

4.2 Study on iliosacral screws

The study on ISS was focused on the influence of positioning of two screws on the stability of the bone. Mechanical response of pelvic stabilisation with a single ISS was not studied as it was proven in other studies not to provide sufficient stiffness and rotational stability [11, 15]. In the two studied cases, dual ISS were applied into S1 vertebra. In ISS-$\parallel$ (see Fig. 1.9d) both screws were located in plane parallel to the sacral base, in ISS-$\perp$ they were positioned along the loading axis, in plane perpendicular to the sacral base (Fig. 1.9e).

Comparing the values of stiffness ratio R presented in Tab. 4.3, significantly higher stiffness of the stabilised model was achieved by the use of ISS-$\perp$. The screw position in this fixation technique reduces both the vertical displacement of the loaded part and the rotation of both bone parts in the frontal plane, resulting in opening of the fracture gap. As a result, the gap remains narrow even in the level of S4 and S5 vertebrae.

This is confirmed by the displacement map displayed in Fig. 4.5b, where it is obvious that the both parts are held together tightly, both displace similarly in vertical direction and no fracture line distraction is observed. Flexion of the sacrum is the dominant movement according to the displacement map as the largest displacements are observed in the frontal part of the bone, ahead of the loading axis.

Contrary to that, the stiffness ratio R of ISS-$\parallel$ was only 0.71. From the displacement maps presented in Fig. 4.5a and Fig. 4.5b it is obvious that the behaviour of ISS-$\parallel$ and ISS-$\perp$ is very different. In case of ISS-$\parallel$, both the screws were positioned in a plane perpendicular to the loading axis and to the fracture line, which did not prevent the distraction of the fracture line. It can be seen in Fig. 4.6 that the relative displacement of bone parts of ISS-$\parallel$ was approximately twice as large as that of ISS-$\perp$.

ISS is the only tested fixator applied directly into the sacral bone while the other fixators are attached to the iliac bones. This fact assures that the fractured bone parts

Tab. 4.3: Stiffness of pelves with ISS fixation technique

Technique	S_I^B [N/mm]	S_F^B [N/mm]	R^B
ISS-$\parallel$	678	481	0.71
ISS-$\perp$	614	562	0.91

are held together at the location of application, which is at the level of S1 vertebra in this study, and almost no relative vertical displacement was allowed.

It can be concluded that better overall results were achieved by using ISS-$\perp$ which provided the bone with higher mechanical stability and the fracture gap did not distract in its lower part as it did in case of ISS-$\parallel$, i.e. the relative rotation of the bone parts was minimised.

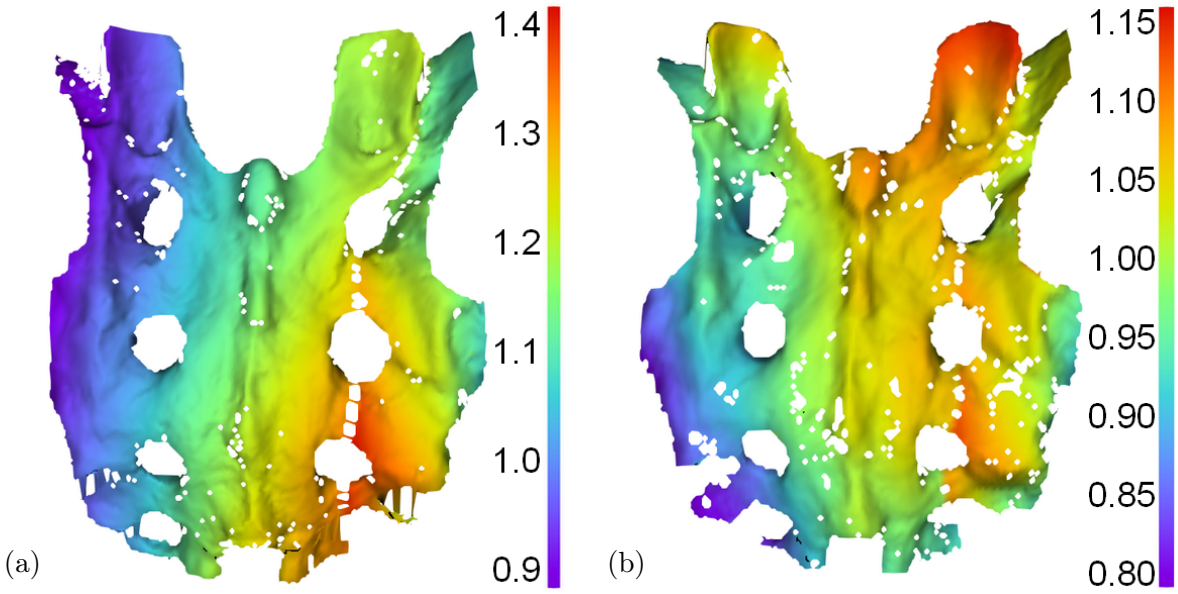

Fig. 4.5: Displacement map of fractured pelvic models stabilised by ISS. Total displacement in mm is displayed. (a) ISS-$\parallel$, (b) ISS-$\perp$.

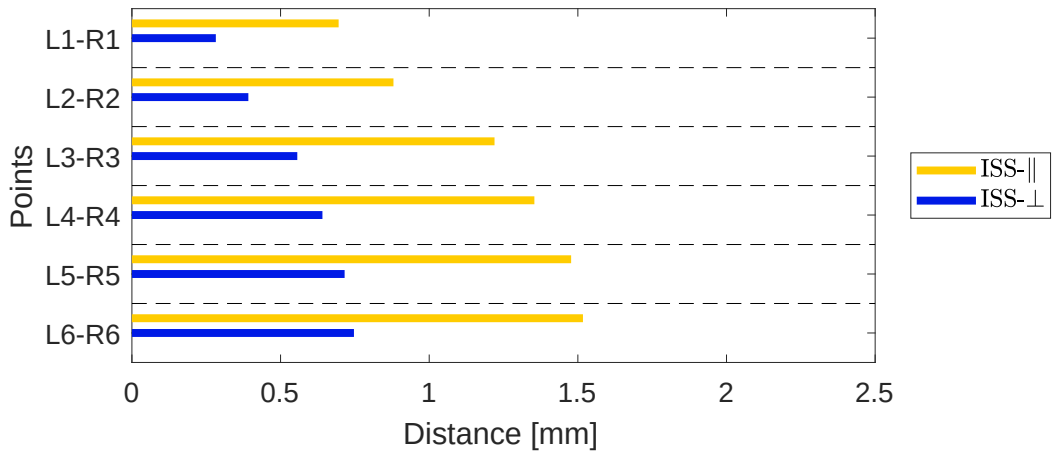

Fig. 4.6: Relative displacement of L-R points for maximal load of models with fracture stabilised by ISS.

However, the possibility of ISS insertion into the sacral vertebrae is a highly individual issue and it must be evaluated for each patient based on the anatomy and inner composition of their sacral bone [8]. In some patients the safe zone in S1 vertebra is not sufficient for the insertion of dual ISS, or its size and shape allow ISS positioning only in a specific way.

4.3 Study on combinations of transiliac internal fixator and iliosacral screw

The combination of TIFI-A and single ISS (Fig. 1.9f) was tested on two pelvic models. In the first case (TFIS-P) the TIFI was accompanied by a partially threaded ISS; in the second case (TFIS-F) a fully threaded ISS was used. The process of application and positioning of the fixators were identical in both cases. The task was to study whether this combined fixation techniques provides better stability in comparison with dual TIFI and dual ISS. In addition, the influence of the thread type was investigated.

The stiffness ratio R for both of the techniques is very similar. Its values – 0.87 for TFIS-P and 0.86 for TFIS-F – suggest that the stiffness of the bone was restored sufficiently by stabilisation using the combination of TIFI and ISS.

Although the stiffness ratio is almost identical, the displacement map of these two techniques differ (see Fig. 4.7). At TFIS-P, the dominant movement is the distraction of the fracture line in its bottom part while the relative displacement of the bone parts is negligible. In the displacement map of TFIS-F the distraction of the fracture line is accompanied by displacement of the loaded part in vertical direction. According to the information obtained from these images, the TFIS-P holds the bone parts together more tightly. In general, TFIS-P also allowed slightly lower relative displacement of the fractured bone parts (see Fig. 4.8).

Tab. 4.4: Stiffness of pelves with TIFI+ISS fixation technique.

Technique	S_I^B [N/mm]	S_F^B [N/mm]	R^B
TFIS-P	547	476	0.87
TFIS-F	542	466	0.86

Considering these results, it can be concluded that the partially threaded ISS (TFIS-P) provides slightly better stability than the fully threaded ISS (TFIS-F); however, the differences between the two techniques are not significant.

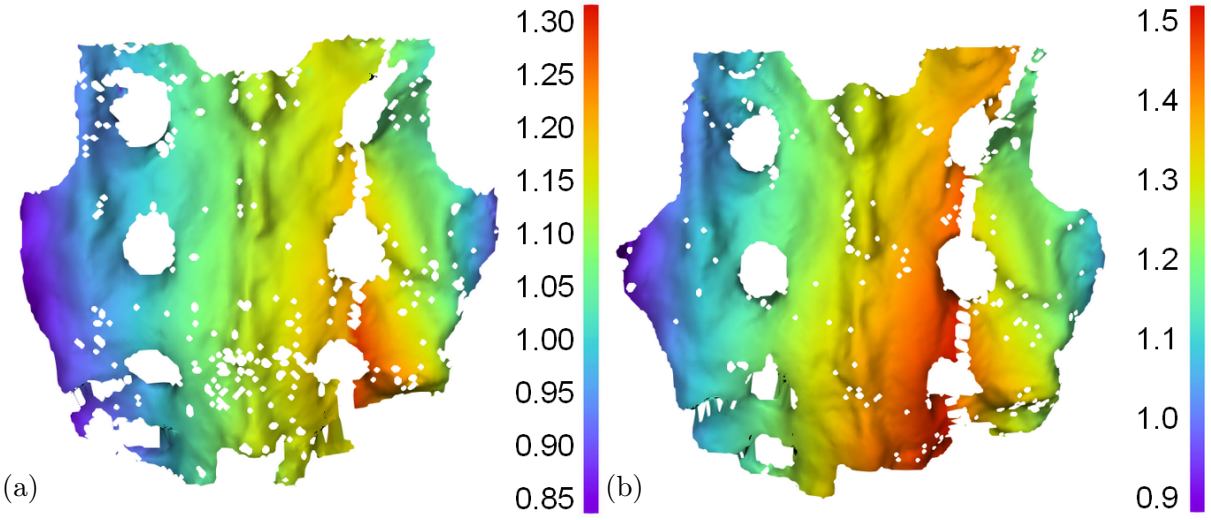

Fig. 4.7: Displacement map of fractured pelvic models stabilised by TIFI and ISS. Total displacement in mm is displayed. (a) TFIS-P, (b) TFIS-F.

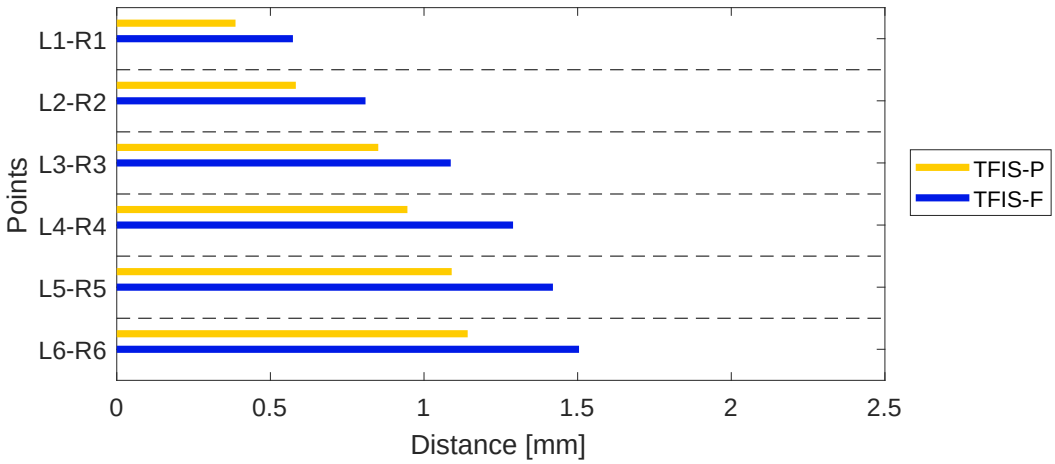

Fig. 4.8: Relative displacement of L-R points for maximal load of models with fracture stabilised by TIFI and ISS.

4.4 Study on sacral bars

One of the studied fixation techniques consisted of two sacral bars, applied craniocaudally into the alae of ilia. The aim of this study was to reveal the influence of the level of compression on the stiffness of the model as it is very challenging issue during the real surgery.

As can be seen in Tab. 4.5, the stiffness ratio R^B for SB-1 is greater than one which means the pelvic model became more stiff after fracturing and stabilisation than in the intact state. The displacement map in Fig. 4.9a suggests that the dominant movement was the flexion of the whole sacrum and the vertical displacement of both parts while the fracture line distraction is not present. The map also reveals that the sides of the fracture were held together very tightly as there is not any visible difference in their vertical displacement along the fracture line. The displacement map is almost symmetric with respect to the sagittal plane, i.e. very similar to the displacement map of intact pelvis presented in Fig. 3.1.

This behaviour was a consequence of an excessive compression of the fracture line which was caused during the application of SB. On one hand, this fixation provided the bone with very high level of stability and achieved great results from the mechanical point of view. On the other hand, the excessive compression is not desirable from the medical point of view as it may lead to pain in the affected area, severe damage to compressed tissues and unfavourable conditions for bone healing.

The same measurement was performed for dual SB with minimal compression on a new pelvic model. An attention was paid to minimise the risk of the undesirable compression and to obtain the pelvic model stabilised in a way suitable for safe treatment, with the appropriate level of compression. In this case (technique SB-2), the stiffness ratio is equal to 0.83. The displacement map presented in Fig. 4.9b reveals that similarly to SB-1, by using SB-2 the sides of the fracture were held together well and moved together mostly

Tab. 4.5: Stiffness of pelves with SB fixation technique.

Technique	S_I^B [N/mm]	S_F^B [N/mm]	R^B
SB-1	536	590	1.10
SB-2	576	478	0.83

vertically. This statement is confirmed by data presented in Fig. 4.10, where it is obvious that for both techniques the relative displacement of the fractured bone parts is very low.

Considering the results of both SB-1 and SB-2, two sacral bars provide the fractured sacral bone with high stiffness ratio and mechanical stability. However, its application is challenging as the assessed level of compression must be optimal for both the safe healing and sufficient mechanical performance.

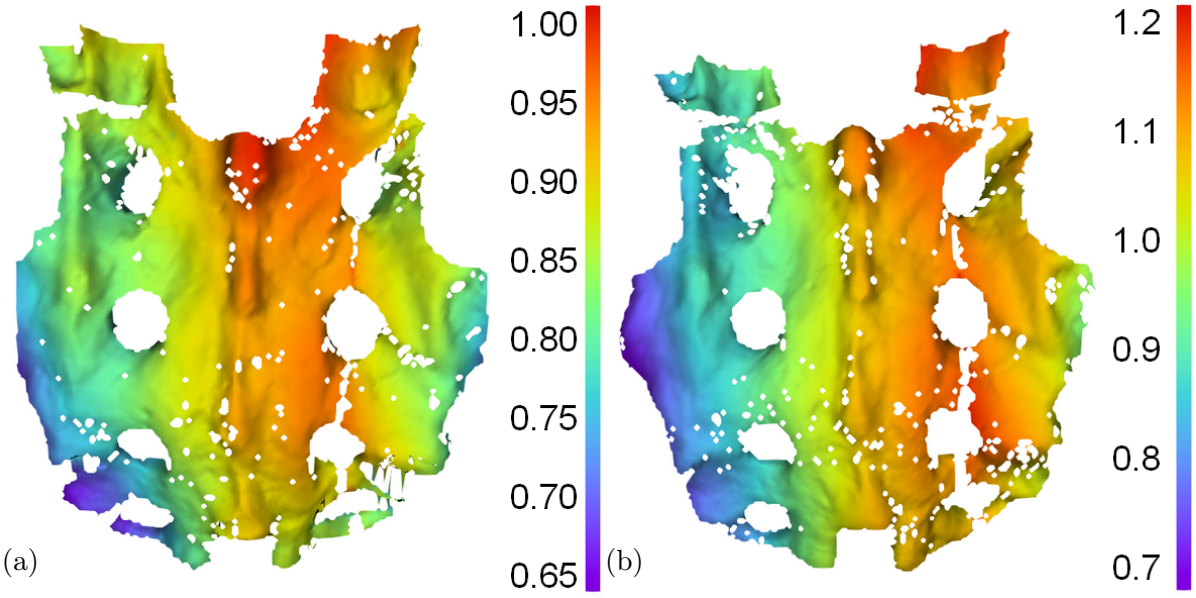

Fig. 4.9: Displacement map of fractured pelvic models stabilised by SB. Total displacement in mm is displayed. (a) SB-1, (b) SB-2.

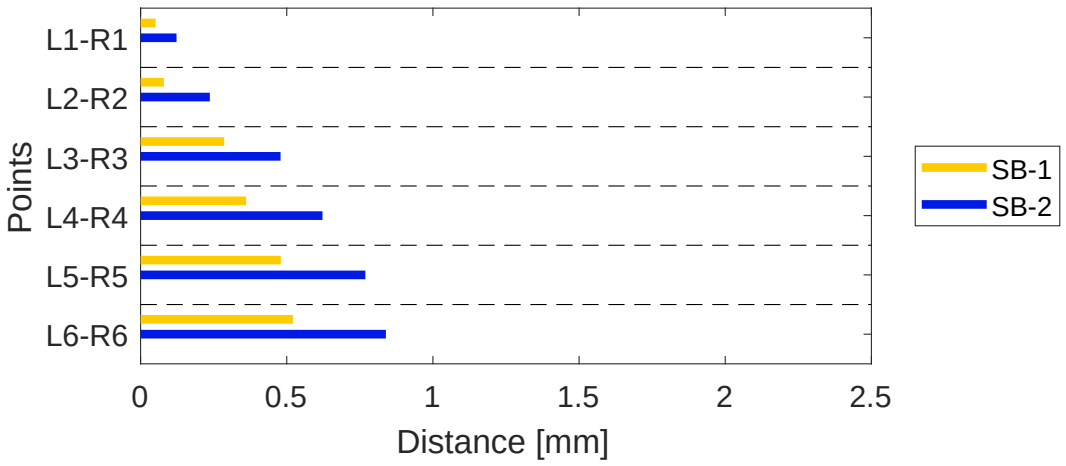

Fig. 4.10: Relative displacement of L-R points for maximal load of models with fracture stabilised by SB.

4.5 Study on transiliac plates

The aim of the study on TP was to study the difference in results achieved by single TP positioned in the level of posterior superior iliac spine, similarly to TIFI-A (TP-S, Fig: 1.9h), and dual TP, where the plates were applied in the same levels as the TIFI-D fixators (TP-D, Fig: 1.9i).

According to the data provided in Tab. 4.6, the stability of these techniques was very similar. Both TP-S and TP-D restored the stiffness of the pelvis to approximately 80 % of its value in the intact state. The displacement maps in Fig. 4.11 reveal that the movements of the bone parts were similar for the both techniques. The fractured bone parts were not held together tightly and a relative displacement of the bone parts is obvious, especially in case of TP-S (Fig. 4.11a and Fig. 4.12). Furthermore, the displacement map of the loaded part suggests the adduction of this part.

These data reveal there is no considerable advantage in the application of second TP to the one positioned in the level of posterior superior iliac spine as the stiffness of the bone is not enhanced by its application. The same conclusion was reached when the TIFI-A and TIFI-D were studied. The transiliac internal fixators were positioned at the same locations as the transiliac plates in corresponding fixation techniques.

Tab. 4.6: Stiffness of pelves with TP fixation technique.

Technique	S_I^B [N/mm]	S_F^B [N/mm]	R^B
TP-S	533	415	0.78
TP-D	541	441	0.81

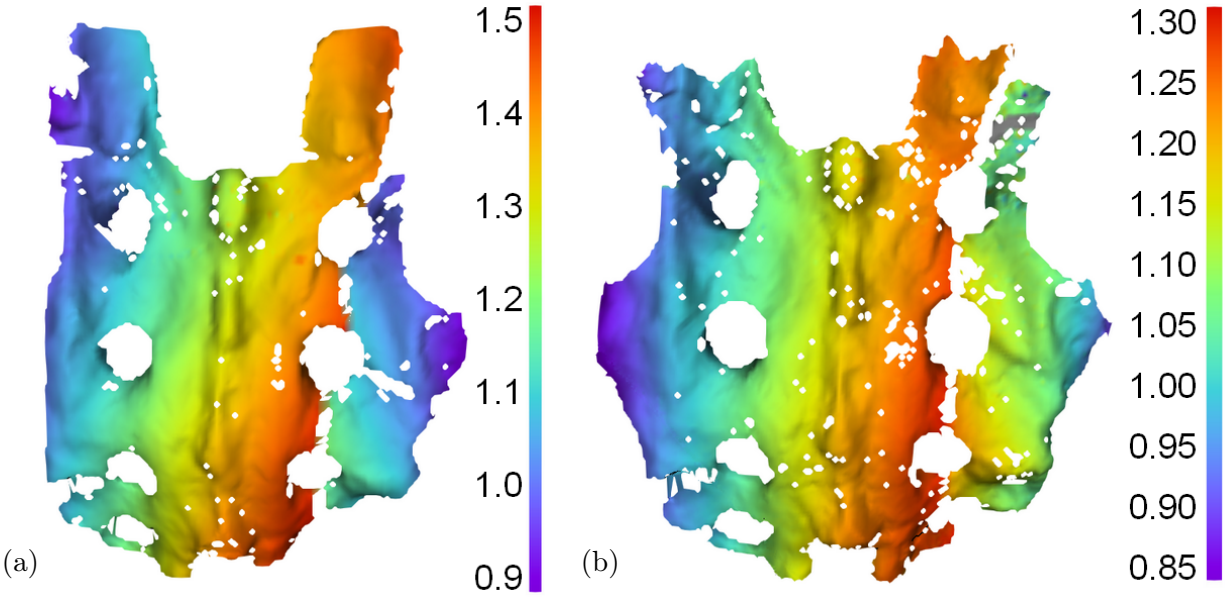

Fig. 4.11: Displacement map of fractured pelvic models stabilised by TP. Total displacement in mm is displayed. (a) TP-S, (b) TP-D.

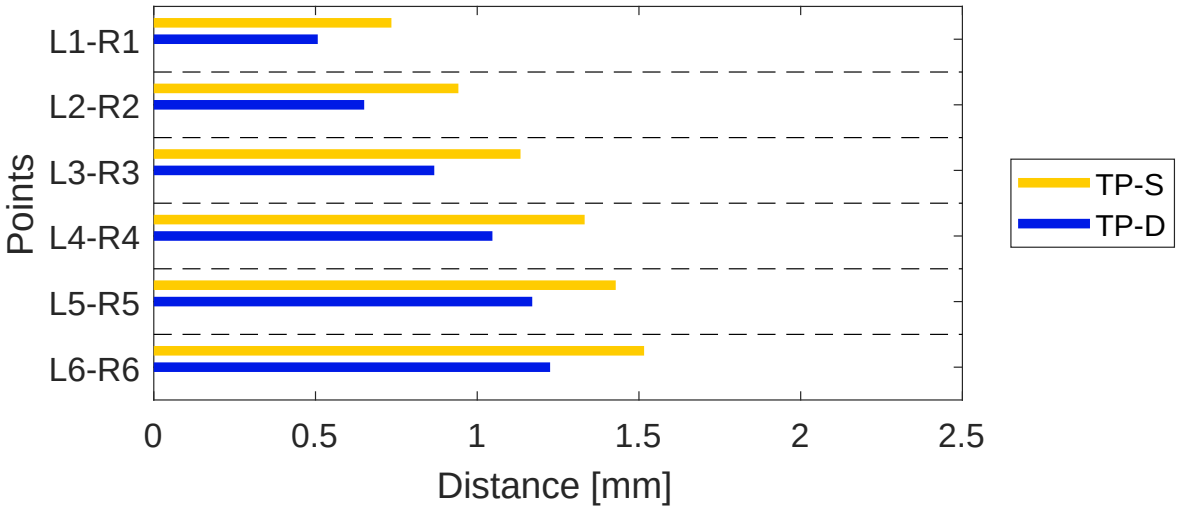

Fig. 4.12: RRelative displacement of L-R points for maximal load of models with fracture stabilised by TP.

4.6 Overall Summary

The studied fixation techniques can be divided into groups according to the level of stiffness provided to the fractured bone. The stiffness ratio of all studied techniques is presented in Fig. 4.13.

To the first group belong techniques which restored the stiffness to at least 85 % ($R^B > 0.85$) of its value in the intact state. These results were achieved by the dual ISS positioned in plane perpendicular to the sacral base and by the combination of TIFI and ISS (for both modifications). By far the highest stiffness ratio was obtained using dual SB. However, including this fixation technique in the first group is questionable as the value of stiffness ratio is related to the excessive compression.

Considering the results of dual SB without excessive compression, this technique would be included into the second group to which belong fixation techniques having the stiffness ratio in the interval from $R^B = 0.75$ to $R^B = 0.85$. This group contains both the dual and the single TP, the dual TIFI and the supraacetabular TIFI.

The lowest level of restored stiffness – under 75 % ($R^B < 0.75$) – was observed for the dual ISS inserted in plane parallel to the sacral base and the application of TIFI at classical position.

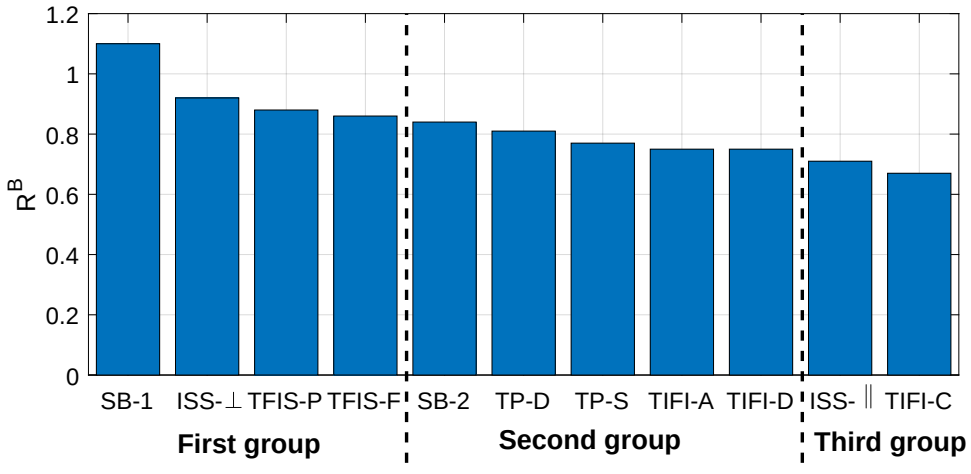

Fig. 4.13: Stiffness ratio of all fixation techniques.

Conclusion

The goal of the thesis was to study the behaviour of fractured sacral bone by the means of experimental and FE analysis. Orthopaedic solid-foam models of human pelvis were subjected to mechanical testing in the material testing machine and their response to the applied load was evaluated. Measurements of models in three states were realised – in the intact state (without any fracture), in the fractured state (fracture was surgically created) and in the stabilised state (fracture was surgically created and subsequently stabilised by particular fixation technique).

During the experimental measurements, a multi-camera DIC system was used for the data acquisition. These data allowed to measure displacements in arbitrary points of the studied sacral surface in each captured step of loading. This information was used in the evaluation of the experimental data.

The data from the experimental measurements performed on the intact and the fractured pelvis were used for the validation of designed FE model of human pelvis. The geometry of the FE model was created using the computed tomography data of the solid-foam model. The solid-foam material properties were determined using tensile tests. Based on these tests, linear isotropic material model was defined in the FE analysis. The FE models of both the intact and the fractured pelvis were created and validated by the corresponding experimental data.

In case of the intact FE model, the difference between the results of the experimental and the FE analysis was lower than 11 % in all of the studied criteria. In case of the fractured model, the results were dependent on the value of the friction coefficient at the foam-to-foam contact interface along the fracture line. Based on all of the evaluation criteria, the FE model corresponded best to the experimental analysis when the friction coefficient $f = 0.8$ was selected. Using this value, the FE model differed from the experi-

ments by less than 11 % in all the evaluated criteria. The experimental determination of the value of the friction coefficient of the solid foam is the subject of further research.

It can be concluded that the behaviour of the FE model is in a good agreement with the experimental results. The model can be further utilised for simulations of more complicated fractures and subsequent testing of the dedicated fixation techniques.

In the experimental study, ten internal fixation techniques for stabilisation of the studied fracture were tested and compared. The evaluation criterion was based on the stiffness of the model provided by the particular fixation technique. The ratio of the stiffness in the stabilised state to the stiffness in the intact state was calculated for each fixation technique.

Furthermore, the DIC analysis of the sacral bone surface enabled both qualitative and quantitative evaluation of bone displacements. In the qualitative analysis, the displacement maps of particular fixation techniques under maximal load were compared and the dominant types of movements of the fractured bone parts were evaluated. In the quantitative analysis, the relative displacements of pairs of points located along the fracture line were determined.

Based on the value of the stiffness ratio, the highest stability was provided by dual SB. However, the results were affected by an excessive compression in the fracture region, which is not desirable in the real surgeries. When the SB fixators were applied with a minimal level of compression, the stiffness ratio of dual SB was significantly lower. These results suggest that the resulting stiffness of the bone is strongly affected by the level of compression.

The study on dual ISS revealed the influence of the positioning of the screws to the provided stiffness. When both the screws were located in a plane parallel to the sacral base (i.e. perpendicular to the loading axis), the stiffness ratio was significantly lower than that of screws positioned in plane perpendicular to the sacral base.

The study of TP led to conclusion that well corresponding results are obtained for dual TP and single TP in the supraacetabular location. The same results were obtained in study of TIFI applied in the same locations. This suggests that there is no need in application of dual TP or TIFI, as the single fixator provides sufficient stability when applied in supraacetabular position. However, a single TIFI in a classical positioning did not reach such good results as the supraacetabular TIFI.

Based on the study of TIFI plus ISS combined fixation technique it provided similar results for both the fully threaded and the partially threaded ISS. The combination of TIFI and ISS provided higher mechanical stability than a single TIFI. The highest mechanical stability was provided by dual ISS positioned craniocaudally.

References

[1] Van de Graaff, K. M. (2002). Human Anatomy, Sixth Edition. Boston: McGraw-Hill.

[2] Gray, H. (1913). Anatomy, Descriptive and Applied. Philadelphia: Lea & Febiger.

[3] Taylor, T. (n. d.). Bones of the Pelvis and Lower Back, InnerBody [on-line]. Available from: http://www.innerbody.com/anatomy/skeletal/lower-torso/pelvis

[4] Hartlová, J. (2015). Experimental analysis of sacral bone fixators (Bachelor thesis).

[5] Pohlemann, T. (2000). Pelvic ring injuries: assessment and concepts of surgical management. In T. P. Rüedi, W. M. Murphy (Eds.), *AO Principles of Fracture Management* (395-418). Davos: AO Publishing.

[6] Trikha, V., Gupta, H. (2011). Current management of pelvic fractures. Journal of Clinical Orthopaedics and Trauma, 2(1): 12-18.

[7] Hauschild, O., Strohm, P. C., Culemann, U., Pohlemann, T., Suedkamp, N. P., Koestler, W., Schmal, H. (2008). Mortality in patients with pelvic fractures: results from the German pelvic injury register. Journal of Trauma-Injury Infection & Critical Care, 64(2): 449-455.

[8] Mendel, T., Noser, H., Kuervers, J., Goehre, F., Hofmann, G. O., Radetzki, F. (2013). The influence of sacral morphology on the existence of secure S1 and S2 transverse bone corridors for iliosacroiliac screw fixation. Injury, International Journal of the Care of the Injured, 44 (12): 1773–1779

[9] Smith, W. R., Ziran, B. H., Morgan, S. J. (Eds.) (2007). Fractures of the Pelvis and Acetabulum. New York: Informa Healthcare USA, Inc.

[10] Levine, A. M. (1997). Fixation of Fractures of the Sacrum. Operative Techniques in Orthopaedics, 7(3): 221-231

[11] Salášek, M. (2014). Minimally invasive stabilization of posterior pelvic ring injuries with a transiliac internal fixator and two iliosacral screws: comparison of outcome and biomechanics (Doctoral dissertation). Retrieved from https://is.cuni.cz/webapps/zzp/detail/112737

[12] Dienstknecht, T., Berner, A., Lenich, A., Nerlich, M., Fuechtmeier, B. (2011). A Minimally Invasive Stabilizing System for Dorsal Pelvic Ring Injuries, Clinical Orthopaedics and Related Research, 469(11): 3209-3217.

[13] Dienstknecht, T., Berner, A., Lenich, A., Zellner, J., Mueller, M., Nerlich, M., Fuechtmeier, B. (2011). Biomechanical analysis of a transiliac internal fixator. International Orthopaedics, 35(12): 1863-1868.

[14] Routt, M. L. C., Simonian, P. T., Inaba, J. (1997). Iliosacral screw complications. Operative Techniques in Orthopaedics, 7(3): 206-220.

[15] Yinger, K., Scalise, J., Olson, S. A., Bay, K. B., Finkemeier, C. G. (2003). Biomechanical comparison of posterior pelvic ring fixation. Journal of Orthopaedic Trauma. 17(7): 481-487.

[16] Banerjee, R., Brink, P.,Cimerman, M., Pohlemann, T., Tomazevic, M. (2016). Pelvic ring – Sacrum [on-line]. Available from *https://www2.aofoundation.org/*

[17] Banerjee, R., Brink, P.,Cimerman, M., Pohlemann, T., Tomazevic, M. (2016). Iliosacral screw for sacrum [on-line]. Available from *https://www2.aofoundation.org/*

[18] Banerjee, R., Brink, P.,Cimerman, M., Pohlemann, T., Tomazevic, M. (2016). Iliosacral screw navigation [on-line]. Available from *https://www2.aofoundation.org/*

[19] Füchtmeier, B., Maghsudi, M., Neumann, C., Hente, R., Roll, C., Nerlich, M. (2004). Die minimal-invasive Stabilisierung des dorsalen Beckenrings mit dem transiliakalen Fixateur interne (TIFI). Der Unfallchirurg, 107(12): 1142-1151.

[20] Gorczyca, J. T., Varga, E., Woodside, T., Hearn, T., Powell, J., Tile, M. (1996). The strength of iliosacral lag screws and transiliac bars in the fixation of vertically unstable pelvic injuries with sacral fractures. Injury, International Journal of the Care of the Injured, 27(8): 561-564.

[21] Chen, B., Zhang, Y., Xiao, S., Gu, P., Lin, X. (2012). Personalized image based templates for iliosacral screw insertions: a pilot study. The International Journal of Medical Robotics and Computer Assisted Surgery, 8(4): 476-482.

[22] Suzuki, T., Hak, D. J., Ziran, B. H., Adams, S. A., Stahel, P. F., Morgan, S. J., Smith, W. R. (2009). Outcome and complications of posterior transiliac plating for vertically unstable sacral fractures. Injury, International Journal of the Care of the Injured, 40(4): 405-409

[23] Majeed, S.A. (1989). Grading the outcome of pelvic fractures. The Journal of bone and joint surgery. British volume, 71(2): 304-306.

[24] McCormick, N., Lord, J. (2010). Digital Image Correlation. Materials Today, 13(12): 52-54.

[25] Sutton, M. A., Orteu, J., Schreier, H. (2009). Image Correlation for Shape, Motion and Deformation Measurements. New York: Springer.

[26] Hartley, R., Zisserman, A. (2003). Multiple view geometry in computer vision. Cambridge: Cambridge University Press.

[27] Dantec Dynamics. Digital Image Correlation. https://www.dantecdynamics.com/digital-image-correlation/

[28] NTIS - New Technologies for the Information Society research centre. *www.ntis.zcu.cz*

[29] Radiology.org (2016). Computed Tomography (CT) – Body [on-line]. Available from: https://www.radiologyinfo.org/en/info.cfm?pg=bodyct

[30] Nordqvist, C. (2017). CT Scan or CAT Scan: How Does It Work? [on-line]. Available from: http://www.medicalnewstoday.com/articles/153201.php

[31] Talpaert, Y. R. (2013). Tensor analysis and continuum mechanics. Dordrecht: Springer Science & Business Media.

[32] Dassault Systemes. Abaqus Unified Fea [on-line]. Available from: https://www.3ds.com/products-services/simulia/products/abaqus/

[33] Dassault Systemes. Abaqus 6.14 [on-line]. Available from: http://abaqus.software.polimi.it/v6.14/

[34] DICOM2FEM [on-line]. Available from: http://sfepy.org/dicom2fem/

[35] Geuzaine, C., Remacle, J. F. (n.d.). A three-dimensional finite element mesh generator with built-in pre- and post-processing facilities [on-line]. Available from: http://gmsh.info/

[36] Altair, HyperWorks. HyperMesh Overview [on-line]. Available from: http://www.altairhyperworks.com/product/HyperMesh/